Climate Determinism Revisited: Multiple Equilibria in a Complex Climate Model

DAVID FERREIRA, JOHN MARSHALL, AND BRIAN ROSE*

Department of Earth, Atmospheric and Planetary Science, Massachusetts Institute of Technology, Cambridge, Massachusetts

(Manuscript received 15 December 2009, in final form 14 October 2010)

ABSTRACT

Multiple equilibria in a coupled ocean–atmosphere–sea ice general circulation model (GCM) of an aquaplanet with many degrees of freedom are studied. Three different stable states are found for exactly the same set of parameters and external forcings: a cold state in which a polar sea ice cap extends into the midlatitudes; a warm state, which is ice free; and a completely sea ice–covered ''snowball'' state. Although low-order energy balance models of the climate are known to exhibit intransitivity (i.e., more than one climate state for a given set of governing equations), the results reported here are the first to demonstrate that this is a property of a complex coupled climate model with a consistent set of equations representing the 3D dynamics of the ocean and atmosphere. The coupled model notably includes atmospheric synoptic systems, large-scale circulation of the ocean, a fully active hydrological cycle, sea ice, and a seasonal cycle. There are no flux adjustments, with the system being solely forced by incoming solar radiation at the top of the atmosphere.

It is demonstrated that the multiple equilibria owe their existence to the presence of meridional structure in ocean heat transport: namely, a large heat transport out of the tropics and a relatively weak high-latitude transport. The associated large midlatitude convergence of ocean heat transport leads to a preferred latitude at which the sea ice edge can rest. The mechanism operates in two very different ocean circulation regimes, suggesting that the stabilization of the large ice cap could be a robust feature of the climate system. Finally, the role of ocean heat convergence in permitting multiple equilibria is further explored in simpler models: an atmospheric GCM coupled to a slab mixed layer ocean and an energy balance model.

1. Introduction

A central question of climate research concerns the existence or otherwise of multiple equilibria. Lorenz (1968, 1970) discusses the implications for climate of whether the governing equations are ''transitive,'' supporting only one set of long-term statistics, or ''intransitive,'' supporting two or more sets of long-term statistics (i.e., multiple equilibria); each of which has a finite probability of resulting from random initial conditions. The proven existence of multiple equilibria in complex models of the climate system would have a profound impact on our interpretation of the paleoclimate record and our perspectives on possible future climates. The paleo record shows that the earth's climate has occupied very different states in the past: for example, ranging from a nearly or completely ice-covered state (snowball earth) during the Neoproterozoic [730–640 million years ago (Ma); e.g., Hoffmann et al. 1998], to a warm house (no ice) in the Cretaceous (e.g., Zachos et al. 2001), to the ''moderate'' present-day climate with ice caps over the poles. Moreover, the paleo record suggests that climate has changed abruptly in the past, particularly during the periods of massive glaciation and deglaciation over the past 2 Ma. Multiple equilibrium states, which might be ''accessed'' suddenly as external forcing parameters slowly change (e.g., orbital parameters, greenhouse gas concentrations, continental drift, etc.) and pass through ''tipping points'' [see the review by Lenton et al. (2008)], could have played a role in such climate excursions. In the context of global climate change in response to anthropogenic greenhouse gas emissions, if multiple equilibria exist then the possibility of massive (and possibly abrupt) climate shifts in response to slow changes would have to be taken very seriously, even if the chance of such an event were very unlikely. Moreover, if the levels of atmospheric greenhouse gases were to be reduced, the climate might not necessarily return to its prior state.

The oceanic and atmospheric literature abounds with studies of simple models that exhibit multiple equilibria

* Current affiliation: Department of Atmospheric Sciences, University of Washington, Seattle, Washington.

Corresponding author address: David Ferreira, EAPS, MIT, Room 54-1515, 77 Massachusetts Avenue, Cambridge, MA 02139. E-mail: dfer@mit.edu

DOI: 10.1175/2010JCLI3580.1

and hysteresis. Among these, two key concepts were formulated by Stommel (1961), who deals with the oceanic thermohaline circulation [or meridional overturning circulation (MOC)],[1] and Budyko (1969) and Sellers (1969), who deal with the ice albedo feedback.

Stommel (1961) found that under certain conditions the MOC could exhibit two stable states: a thermal mode with vigorous circulation and a haline mode with weak circulation. This concept has raised a considerable interest, as evidenced by the extensive literature on the subject, in part because it was linked to the paleoclimate record (Broecker et al. 1985). The mechanism and the historical development of Stommel-type models are reviewed by Stocker (1999).

The present results pertain to the body of work exploring ice albedo feedback, which goes back to the energy balance models (EBMs) of Budyko (1969) and Sellers (1969). These models treat the competing effects of meridional energy transport and local radiative processes on surface temperature and provide an elegant representation of the nonlinear ice albedo feedback. One of the hallmarks of this feedback is the existence of two very different equilibrium climates for a given solar forcing: a warm climate with a small ice cap (or none at all) and a very cold, completely ice-covered snowball. Between the two stable equilibria lies a third solution with large but finite ice cover. However, in the classical EBM, this large ice cap is unstable to small perturbations and is thus not a physically realizable state. The early EBM literature is reviewed by North et al. (1981).

Recently, Rose and Marshall (2009, hereafter RM09) proposed a significant extension of classical EBMs, which allows them to maintain a large stable ice cap extending down in to middle latitudes. The key additional processes are the inclusion of (i) latitudinal structure in the meridional ocean heat transport (OHT) with minima at which the ice edge can rest and (ii) the insulating effect of sea ice on the underlying ocean. The resulting model supports three stable states: a solution with a large ice cap extending down to middle latitudes, a small ice cap, and the snowball. The stable large ice cap state is absent from the classical EBM, because the implied OHT in the latter has a broad hemispheric structure, a sinusoidally shaped bump extending from equator to pole, very much like the atmospheric energy transport but unlike observed OHT (see, e.g., estimates by Trenberth and Caron 2001).

Although the multiple equilibrium properties of EBMs (and Stommel's model) are well understood, one must be cautious in extrapolating from simple models, which allow only a few degrees of freedom, to more complex models and thence to the real climate, which has many, many degrees of freedom. For example, Lee and North (1995) show that some otherwise stable EBM solutions can be rendered unstable with the addition of noise representing the internal variability of an atmospheric general circulation model (GCM). Indeed, hitherto, the existence of multiple stable states has not been conclusively demonstrated in complex coupled climate models.

In GCMs, multiple states of the MOC can be revealed through "water hosing" experiments in which freshwater perturbations are added to the high latitudes of the North Atlantic basin. Typically, the MOC collapses for some finite freshwater anomaly and does not recover its initial state once the anomaly is reduced. Manabe and Stouffer (1988) were the first to report on such multiple states in a coupled ocean–atmosphere–sea ice GCM. However, they employed surface salt flux adjustments, an acceleration technique for the ocean convergence (Bryan 1984), which creates spurious sources of heat/salt in the ocean interior; a coarse resolution (R15), which prevents the development of synoptic-scale eddies; an annual-mean insolation; and a prescribed annual-mean cloud cover derived from observations. All these features were required to carry out such an experiment at the time, but they raise major questions about the robustness of the result.[2] Following Manabe and Stouffer (1988), multiple states of the MOC under water-hosing forcing were extensively studied in ocean-only models (e.g., Rahmstorf 1995) and more recently in coupled GCMs (Rahmstorf et al. 2005; Stouffer et al. 2006). Rahmstorf et al. (2005) report on a standardized water-hosing intercomparison project with earth system coupled models of intermediate complexity. They find that all coupled GCMs exhibit multiple states of the MOC. Although the study includes a wide variety of GCMs, all calculations are compromised by at least one of the following two limitations: 1) freshwater/heat/momentum flux adjustments and 2) use of a simplified atmosphere (EBM, zonally averaged, or statistical model). As in Manabe and Stouffer (1988), flux adjustment breaks the laws of conservation in the coupled climate system and results in air–sea fluxes inconsistent with the oceanic and atmospheric dynamical transports. The use of a simplified atmosphere, on the other hand, effectively reduces the coupled system to a low-order system. Additionally, it suppresses the development of a vigorous storm track and hence the energizing of a substantial internal variability

[1] The notion of multiple equilibria in the abyssal ocean circulation is actually much older, dating back to Chamberlin (1906).

[2] Manabe and Stouffer were the first to recognize this, they say: "In this study, it was necessary to adjust the rate of water exchange at the ocean–atmosphere interface in order to remove a systematic bias of the model. In view of this artificial adjustment of surface water flux, one has to regard the present results with caution."

in the coupled climate system. As mentioned above, the presence of noise could lead to the destabilization of otherwise stable equilibria. From a dynamical point of view, the absence of atmospheric eddies requires parameterization of the meridional transports and surface winds. The use of a simplified atmosphere also often requires ad hoc choices about air–sea coupling (e.g., the zonal repartition of precipitation).

In a water-hosing intercomparison similar to that of Rahmstorf et al. (2005) but with more comprehensive coupled GCMs, Stouffer et al. (2006) report possible multiple equilibria in only two cases. However, these are not run out to steady state and employ surface flux adjustment (and in one case an EBM atmosphere).

Investigation with GCMs of the multiple states due to the ice albedo feedback is scarcer. Langen and Alexeev (2004) found multiple equilibria, including stable large ice caps, in an atmospheric GCM coupled to a mixed layer ocean with a thermodynamic sea ice model and prescribed OHT. The latter, of course, is a major caveat, because it decouples key elements that interact with one another in the climate system. This study also neglects the seasonal cycle of solar forcing, thus missing a key source of potentially destabilizing variability. The existence of the snowball state as a multiple equilibrium alongside a nearly ice-free state, which is the primary prediction of the classical EBM, has recently found support by Marotzke and Bozet (2007) in a state-of-the-art coupled GCM configured for the present day. However, a steady-state snowball is artificially achieved by limiting the growth of sea ice thickness to 8 m (this is effectively equivalent to a spurious heat source to prevent the ''runaway'' freezing of all water). That said, it remains unclear whether the climate system can also support stable intermediate states with large but finite ice caps. There is evidence that the convergence of OHT plays a key role in limiting sea ice expansion, both in the observed modern climate (Bitz et al. 2005) and in modeling studies of the approach to a snowball (e.g., Poulsen et al. 2001).[3]

Here, we report that a complex coupled ocean–atmosphere–sea ice climate model with many degrees of freedom supports three multiple equilibrium states akin to the simple model solutions in RM09. The context of our calculations is that of the aquaplanet, a planet just like our own with an atmosphere and ocean, except that the geometrical constraints on ocean circulation are reduced to a minimal description: the land is represented by a sequence of sticks as described in Marshall et al. (2007), Enderton and Marshall (2009), and Ferreira et al. (2010). Multiple equilibria are found in two different land configurations: the pure aquaplanet, ''Aqua,'' in which topographic constraints are absent from both fluids as the ocean covers the entire globe and the ''Ridge'' setup in which a strip of land extends from pole to pole. We will see that both configurations exhibit three stable states: a warm climate (no ice), a cold climate (ice extending down to about 50°), and a snowball. The sea surface temperature (SST) and sea ice thickness of the warm and cold states are illustrated in Fig. 1.

We emphasize from the outset that the computations reported here include three-dimensional (3D) dynamics in both ocean and atmosphere (and eddy resolving in the latter), do not depend on artificial forcing or flux adjustments and that all solutions are integrated out to equilibrium. The main result of the present study is twofold: 1) a complex, dynamically consistent coupled climate GCM with vigorous internal variability and including the seasonal cycle can support multiple equilibrium states and 2) in addition to the extreme snowball and (nearly) ice-free states, a third equilibrium with a large, finite ice cap is permitted. This is made possible by the meridional structure in OHT, as anticipated in RM09's EBM.

We argue here that the complexity (and consistency) of the physics included in our coupled GCM represent a significant improvement over previous studies of multiple states. The simplified geometries however are a caveat although the existence of multiple states in two very different setups encourages us to think that our results are not just an exotic consequence of a particular geometry.

Our paper is set out as follows: In section 2, we present a brief description of the coupled model. In section 3, the multiple equilibria are described, emphasizing the common aspects of the Ridge and Aqua configurations. An atmospheric model coupled to a slab mixed layer ocean with prescribed OHT is used, in section 4, to explore the role of the OHT meridional structure in the multiple states. In section 5, we modify RM09's EBM to interpret the GCM results emphasizing the key physics at play. In section 6, we conclude.

2. Description of the coupled GCM

We use the Massachusetts Institute of Technology general circulation model (MITgcm) in a coupled ocean–atmosphere–sea ice setup (Marshall et al. 1997a,b). The model exploits an isomorphism between ocean and atmosphere dynamics to generate atmosphere and ocean models from the same dynamical core (Marshall et al.

[3] For completeness, we note a third type of multiple states found in GCMs: multiple equilibria of the biome–atmosphere coupled system (Claussen 1998; Wang and Eltahir 2000; Renssen et al. 2003). In these studies, there is either no dynamical ocean or a minimal role for the ocean. The impact of these multiple states on climate is strongest at continental scale (usually over North Africa and central East Asia) and is weak at the global scale.

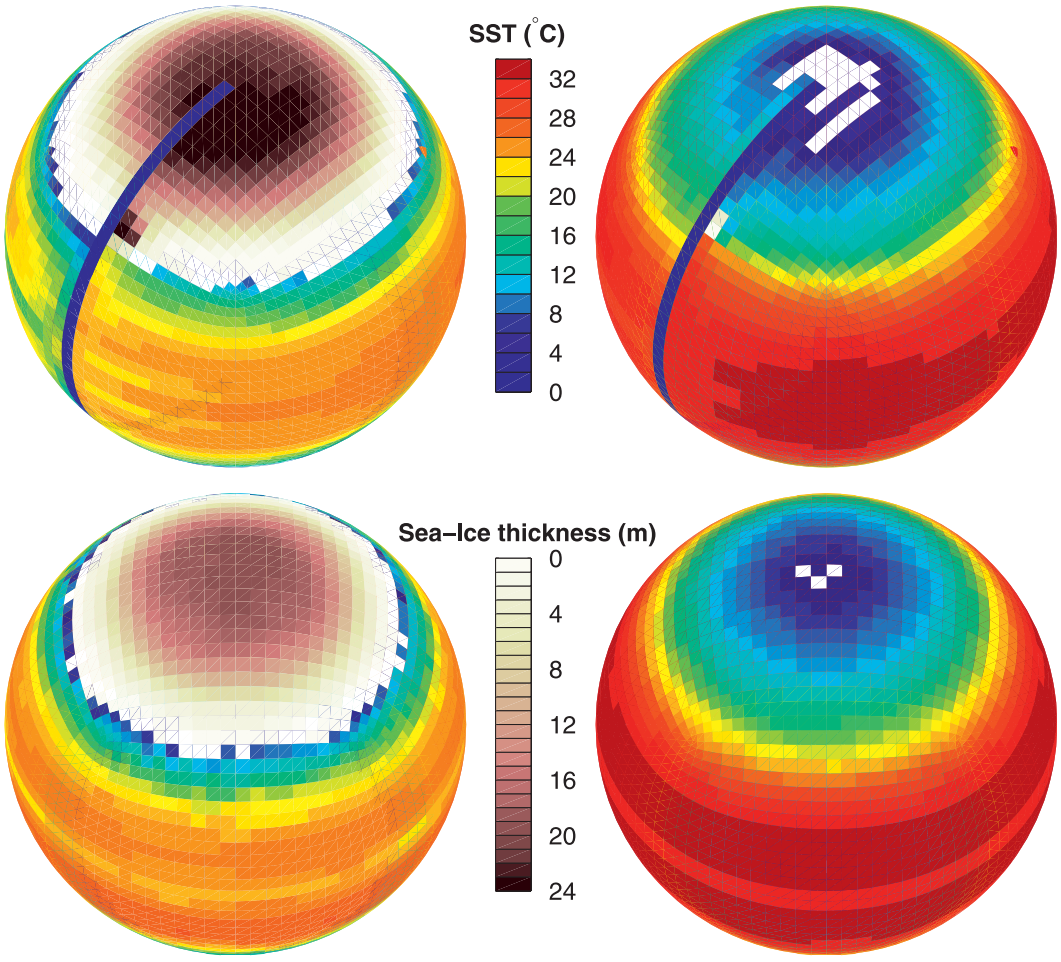

FIG. 1. SST and sea ice thickness in (top) Ridge and (bottom) Aqua for the (left) cold and (right) warm solutions.

2004). The model uses the following vertical coordinates: the pressure coordinate p for the compressible atmosphere and the rescaled height coordinate z^* for the Boussinesq ocean (Adcroft and Campin 2004). As described in Adcroft et al. (2004), both component models use the same cubed-sphere grid at a low resolution C24 (24×24 points per face, yielding a resolution of 3.75° at the equator). The cubed-sphere grid avoids problems associated with converging meridians at the poles and ensures that the model dynamics there are treated with as much fidelity as elsewhere. Additionally, it greatly simplifies the implementation of a conservative interface between ocean and atmosphere (see Campin et al. 2008).

The atmospheric model is based on the Simplified Parameterizations, Primitive-Equation Dynamics (SPEEDY) physics scheme (Molteni 2003). Briefly, it comprises a four-band radiation scheme, a parameterization of moist convection, diagnostic clouds, and a boundary layer scheme (see discussions in Molteni 2003; Marshall et al. 2007). A low vertical resolution is employed: one level is placed in the boundary layer, three are placed in the troposphere, and one is placed in the stratosphere. The 3-km-deep, flat-bottomed ocean model has 15 vertical levels, increasing from 30 m at the surface to 400 m at depth. Effects of mesoscale eddies are parameterized as an advective process (Gent and McWilliams 1990) together with an isopycnal diffusion (Redi 1982), both with a transfer coefficient of 1200 $m^2\ s^{-1}$. Convective adjustment, implemented as an enhanced vertical mixing of temperature and salinity, is used to represent ocean convection, as described in Klinger et al. (1996). The background vertical diffusion is uniform and set to a value of $3 \times 10^{-5}\ m^2\ s^{-1}$. A nonlinear equation of state is employed (Jackett and McDougall 1995).

A sea ice model is included based on the Winton (2000) two and a half layer thermodynamic model. The prognostic variables are ice fraction; snow and ice thickness; and a two-level enthalpy representation, which accounts for brine pockets and sea ice salinity, employing an energy conserving formulation. There is no sea ice dynamics.

However, we use a diffusion of sea ice thickness as a proxy for ice dynamics.[4] The snow-albedo parameterization (also used for snow over land[5]) depends on snow height, surface temperature, and the age of the snow (a detailed description is given in appendix A). The atmospheric CO_2 level is prescribed at present-day values. The seasonal cycle of insolation is represented (using a present-day obliquity of 23.5° and zero eccentricity), but there is no diurnal cycle. The setup is identical to that used in Ferreira et al. (2010) and very similar to that used in Marshall et al. (2007) and Enderton and Marshall (2009); for key differences, see Ferreira et al. (2010).

The coupled system can be integrated for 1100 yr in one week of dedicated computer time. Fluxes of momentum, freshwater, heat, and salt are exchanged every hour (the ocean time step). Finally, as discussed by Campin et al. (2008), our model does not require an artificial limit on sea ice thickness to avoid the drying out of the ocean cells. This is made possible by the use of the z^* coordinate. This, in addition, allows for a realistic treatment of the sea ice–ocean interface. Our coupled ocean–atmosphere–sea ice model thus achieves perfect (machine accuracy) conservation of freshwater, heat, and salt during extended climate simulations, a property which is crucial to the fidelity and integrity of the coupled system.

3. Description of multiple equilibrium states

For each of the Aqua and Ridge configurations, three equilibrium states have been found that use exactly the same set of parameters (and in fact are run from the same executable file). The only external forcing is due to incoming solar radiation and the prescribed level of CO_2. In particular, air–sea heat fluxes are fully consistent with the ocean and atmosphere energy/mass transports, because the model employs a real freshwater formulation, even in the presence of sea ice (see Campin et al. 2008), and there are no flux adjustments. Our solutions are fully equilibrated and do not exhibit any drift, despite significant variability. Moreover, after reaching statistical equilibrium, they were run out for a further thousand years or more. The last 4100 yr of the global volume-averaged ocean temperature for each run are shown in Fig. 2. Note that the time series were shifted so that they could all fit within 1°C and some of the very long time scale variability can be seen.

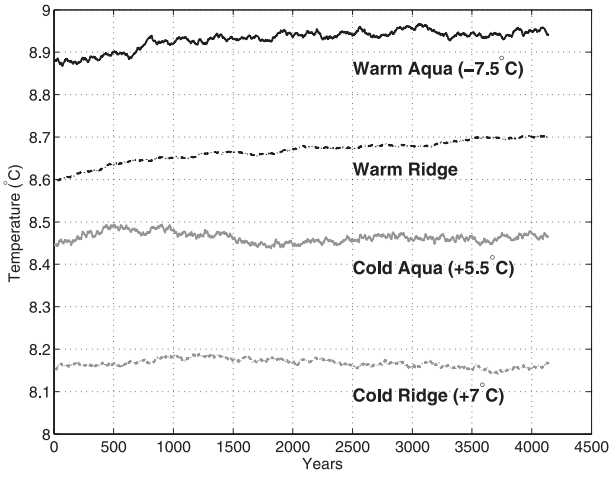

FIG. 2. Time series of the global volume-averaged temperature of the ocean in the four simulations. The last 4100 yr are shown. Note that the time series of the warm Aqua, cold Aqua, and cold Ridge are shifted (the shift is indicated in parentheses), but the ordering of the global mean temperatures is preserved: converged values for the warm Aqua, warm Ridge, cold Aqua, and cold Ridge are 16.44°, 8.7°, 2.96°, and 1.15°C, respectively.

Aqua uses a solar constant $S_o = 1366\ \mathrm{W\ m^{-2}}$ (the modern value) but slightly different sea ice–albedo parameters than the reference configurations presented in Marshall et al. (2007), Enderton and Marshall (2009), and Ferreira et al. (2010). Ridge, on the other hand, uses the reference albedo parameters but a slightly lower solar constant value of $1352\ \mathrm{W\ m^{-2}}$. Values of the albedo parameters are given in Table 1 and appendix A.

The differing solar constants are a product of the procedure to find the multiple states. The multiple states in Aqua were in fact discovered inadvertently in the process of exploring the sensitivity of the solutions to the ice/snow and ocean albedos. In light of this result and the study of RM09 (who considered the role of ocean gyres in shaping the structure of the OHT), we searched for multiple states in Ridge in a more systematic way. Starting from the reference (ice free) Ridge simulation (Ferreira et al. 2010), the solar constant was slowly decreased until a large ice cap appears and stabilizes at $S_o = 1352\ \mathrm{W\ m^{-2}}$. Solutions for intermediate solar constants exhibited tendencies to drift back to an ice-free state: one of them was carried forward and its solar constant readjusted to $S_o = 1352\ \mathrm{W\ m^{-2}}$.

TABLE 1. Table of the ice/snow albedo parameters. See appendix A for definitions.

	$\alpha_I^{\max}$	$\alpha_I^{\min}$	α_S^{cold}	α_S^{warm}	α_S^{old}
Aqua	0.7	0.30	0.85	0.5	0.5
Ridge	0.6	0.25	0.80	0.45	0.45

[4] The Aqua calculation was repeated without diffusion of sea ice thickness. The results do not change substantially; multiple equilibria are found both with and without sea ice thickness diffusion.

[5] Although the land surface plays a negligible role in Ridge (because of its small width), we nevertheless solve for temperature, soil moisture, and runoff associated with the land cells.

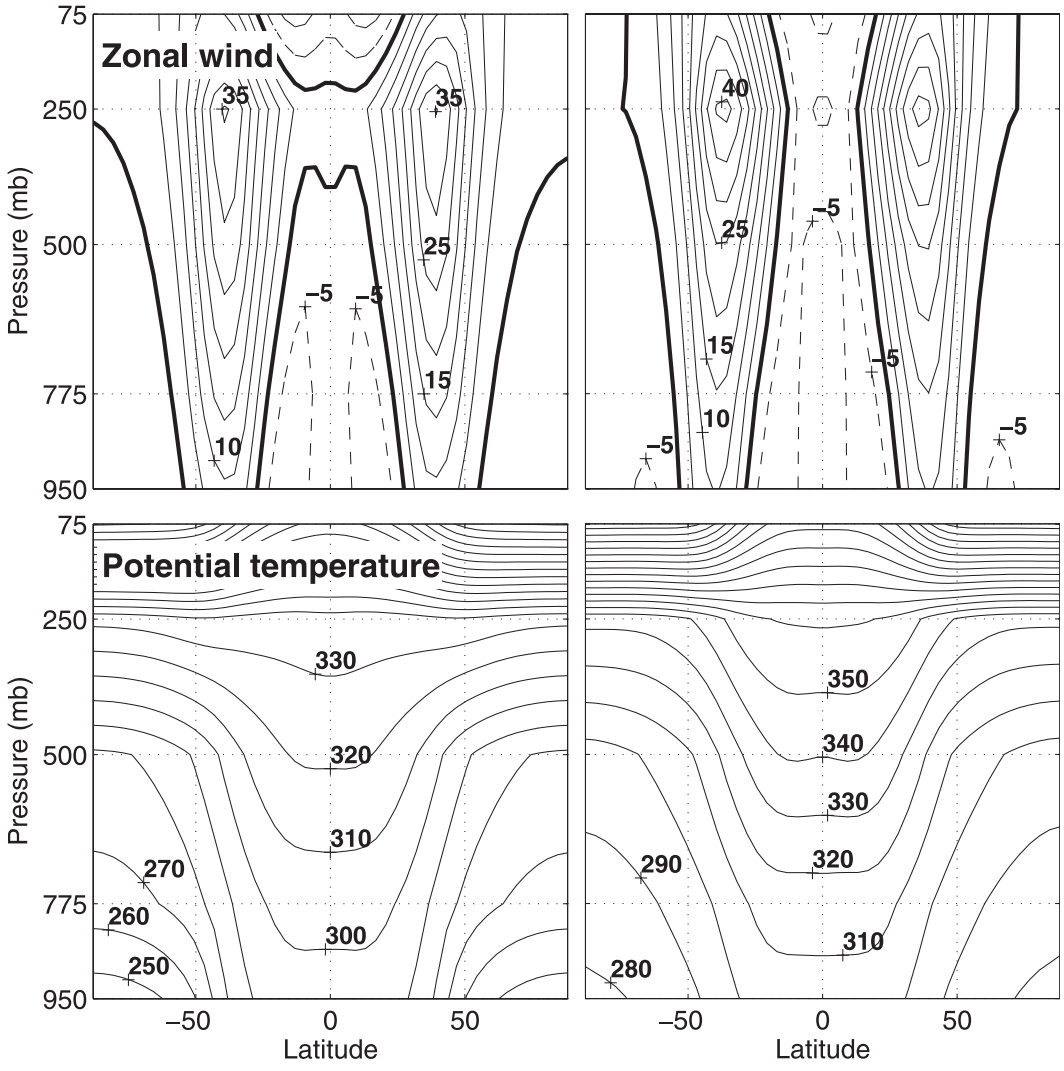

FIG. 3. Zonally averaged (top) zonal wind (m s^{-1}) and (bottom) potential temperature (K) for the (left) cold and (right) warm solutions of Ridge. For the wind, the solid and dashed contours denote westward and eastward flow, respectively, and the zero contour is highlighted. The Aqua atmospheric states are very similar.

As might be anticipated from a consideration of EBMs, a snowball solution exists for both Ridge and Aqua. These states are not our primary focus of attention here but are briefly described in appendix C. Of the two other equilibria, one is warm (with ice only at the very pole) and one is cold (with ice extending down to middle latitudes). We refer to these as the warm and cold solutions, respectively.

All solutions presented here are nearly symmetric about the equator, reflecting the symmetric boundary conditions of both Aqua and Ridge. Attempts to find asymmetric states (e.g., ice in only one hemisphere) by integrating from asymmetric initial conditions have thus far been unsuccessful. Asymmetric geometrical constraints, as seen in realistic geography, could be important to obtain asymmetric states.[6]

a. Atmospheric state

Figure 3 shows the zonal wind and potential temperature for the cold and warm atmospheric states of Ridge. The corresponding solutions in Aqua are very similar to

[6] Note that asymmetric ocean states such as those found by Bryan (1986) are unlikely in a coupled system. They were obtained in an ocean-only experiment under a prescribed surface freshwater flux symmetric around the equator. In a coupled system, an asymmetric ocean circulation would lead to asymmetries in SST, atmospheric state, and eventually evaporation minus precipitation.

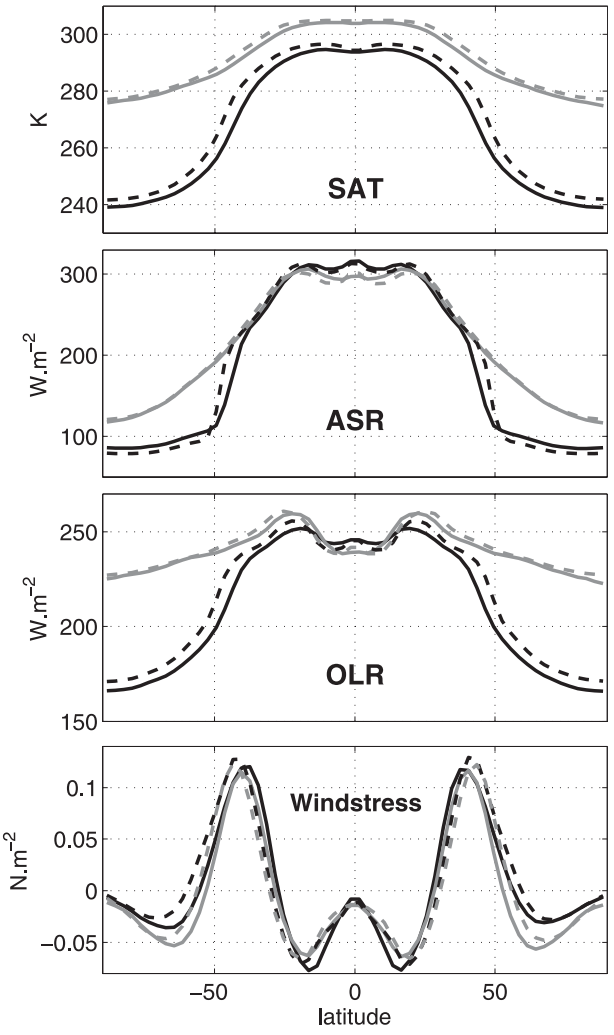

FIG. 4. (top)–(bottom) Surface air temperature, TOA ASR, TOA OLR, and surface wind stress for the cold (black) and warm (gray) solutions of Ridge (solid) and Aqua (dashed).

those in Ridge and are therefore not shown [Fig. 4, however, presents zonal-average plots of surface air temperature, surface zonal wind stress, and top-of-the atmosphere (TOA) outgoing longwave radiation (OLR) and absorbed shortwave radiation (ASR) fluxes for both Aqua and Ridge]. Note that Figs. 3–7 of the coupled GCM are 40-yr averages. The zonal winds of the warm and cold states have generally similar patterns and magnitudes, with trade winds in the tropics, westerly winds centered around 40°, and subpolar easterlies north of 55°. The temperature structures are also similar with flat isotherms in the deep tropics and broad baroclinic zones (in thermal wind balance with the zonal winds) in mid- to high latitudes. There are some noteworthy differences, however. The jet stream is slightly broader in the cold state with weaker polar easterlies and slightly stronger trade winds. This is probably because of the presence of sea ice, which generates strong meridional temperature gradients at low levels (see bottom-left panel near 60°) and thus strengthens and extends the baroclinic zone poleward into high latitudes. The eddy heat flux $\overline{v'T'}$ in the storm track (computed from bandpassed anomalies between 2.5 and 10 days) has a broader meridional extent and is more intense in the cold than in the warm state. This latter effect contributes significantly to the larger atmospheric heat transport (AHT) at those latitudes in the cold state (see Fig. 6).

In the upper troposphere, meridional temperature gradients are weaker in the cold state because of a weaker stratification in the deep tropics. This is associated with a larger tropical lapse rate (which closely follows a moist adiabat) found in colder/drier climates: the equatorial lapse rate is 6.4°C km^{-1} in the cold state compared to 5.3°C km^{-1} in the warm state. The weaker meridional gradient in the upper troposphere in the cold state counteracts the stronger gradient at low levels. This leads to the somewhat counterintuitive result that upper-level westerlies are larger in the warm state than in the cold one. The strength of the surface winds does not change noticeably between the warm and cold states, however (see Fig. 4).

b. Oceanic state

Figure 5 shows the time- and zonal-mean ocean temperature and the residual-mean overturning circulation for the cold and warm states of Ridge and Aqua. In both states, the temperature exhibits a marked thermocline in the subtropics because of pumping down of warm water from the Ekman layer around 25°N/S and upward suction of cold water at the equator and near 50°N/S, reflecting the pattern of surface wind stress. Despite broad similarities in their thermal structures, Ridge and Aqua exhibit very different dynamical balances. The meridional barrier in Ridge allows both zonal pressure gradients and geostrophic meridional currents to contribute to balancing the applied wind stress. A gyre circulation develops with a Sverdrup interior, western boundary currents, and marked zonal asymmetries. The thermocline is relatively shallow. In Aqua, however, the thermocline is deep: the zonal stress is balanced by (parameterized) eddy form stress, as described in Marshall et al. (2007), following the model of the Antarctic Circumpolar Current developed by Marshall and Radko (2003).

In the warm states, there is also a thermocline at high latitudes (poleward of 50°) due to the presence of polar easterlies, which act to pump freshwater (~28 psu) down from the surface, creating very stable stratification. In the cold state, sea ice exists poleward of 50° or so. Here, SSTs are uniform and close to −1.9°C. Those cold dense waters extend over the whole high-latitude water column

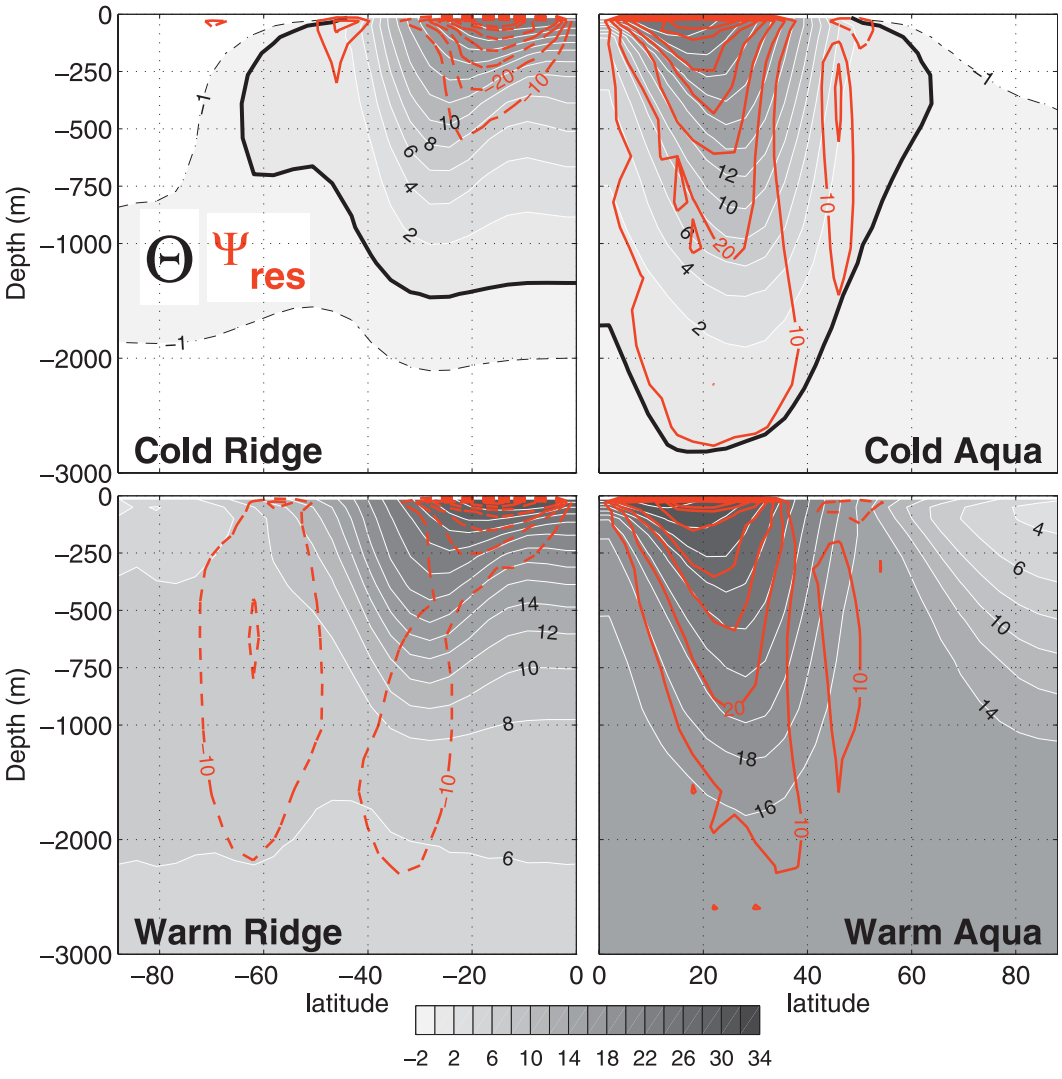

FIG. 5. Zonally averaged potential temperature (gray shading) and Ψ_{res} (red) in the ocean for the (top) cold and (bottom) warm solutions of (left) Ridge and (right) Aqua. For temperature, the contour interval is 2°C, while the dashed and thick solid lines highlight the −1° and 0°C contours, respectively. The residual-mean circulation (Sv) is the sum of the Eulerian and eddy-induced circulation. Solid and dashed contours denote clockwise and anticlockwise circulations, respectively. Because the solutions are symmetric about the equator, only one hemisphere is shown.

and cover the bottom of the ocean. In the warm states, deep temperatures are much higher, by a full 7° and 15°C relative to the cold state in Ridge and Aqua, respectively.

In all solutions, the temperature of bottom water is close to that of the surface waters at the poleward edge of the subtropical thermocline, around 50°–55°N/S. In Aqua, this is straightforward to understand, because deep convection occurs near 50°, where isopycnals are drawn upward by Ekman suction and weak stratification develops in subsurface layers (a phenomenon similar to preconditioning; see the review in Marshall and Schott 1999). In Ridge, deep convection occurs on the eastern side of the basin between 60° and 80° of latitude. However, because of advection by the subpolar gyre, relatively warm surface waters present at the gyre boundary are advected eastward and poleward into the convective region. In both warm and cold states, the temperature of deep water does not correspond to the coldest water at the surface but rather to the somewhat higher temperature typical of surface waters near 50°–55°N/S.

In all solutions, the residual-mean circulation is dominated by the subtropical wind-driven cells, although the pattern of overturning differs strongly between Ridge and Aqua, reflecting the different dynamics at play. In particular note the deep overturning cell in Aqua extending over the thermocline. Here the quasi adiabaticity

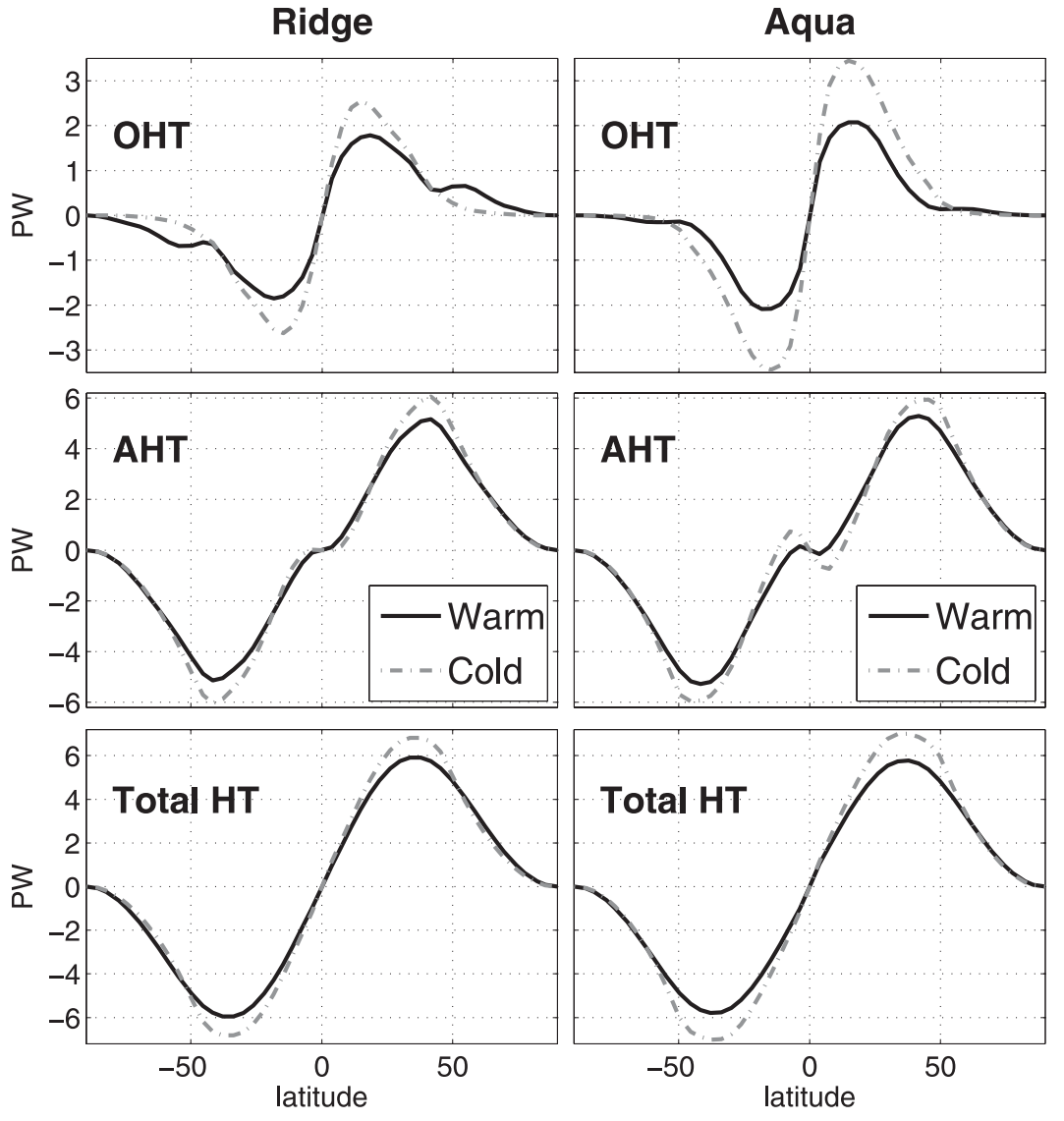

FIG. 6. (top) Oceanic, (middle) atmospheric, and (bottom) total heat transport for the cold (dot-dashed) and warm (solid) solutions of (left) Ridge and (right) Aqua (PW = 10^{15} W).

of the circulation in the ocean interior is clearly revealed by the coincidence of streamlines and isotherms (note that density is dominated by temperature in the subtropics). In Ridge, this is less evident because of zonal asymmetries in the ocean state.

The pattern and magnitude of the overturning circulation changes little between the cold and warm states, consistent with the fact that they are primarily wind driven and the broad pattern of surface winds changes little. A notable exception is the disappearance of the high-latitude cell in the cold solution of Ridge with the growth of the sea ice cap. In the warm state, this cell is associated with deep convection and deep-water formation at these latitudes.

c. *Meridional energy transports*

The ocean, atmosphere, and total (atmosphere plus ocean) heat transports are shown in Fig. 6. The OHT reaches a maximum in the subtropics near 20°N/S, where it dominates the total transport, and becomes small at high latitudes. Because of the ridge, which supports a subpolar gyre and high-latitude deep convection, the OHT in the warm state of Ridge has a small, albeit significant, contribution poleward of 50°. In comparison, the AHT has a smoother, hemispheric-scale structure with maxima at 45°N/S.

The OHT scales as $\sim\Psi\Delta T$, where Ψ is the strength of the MOC and ΔT is the (vertical) difference in potential

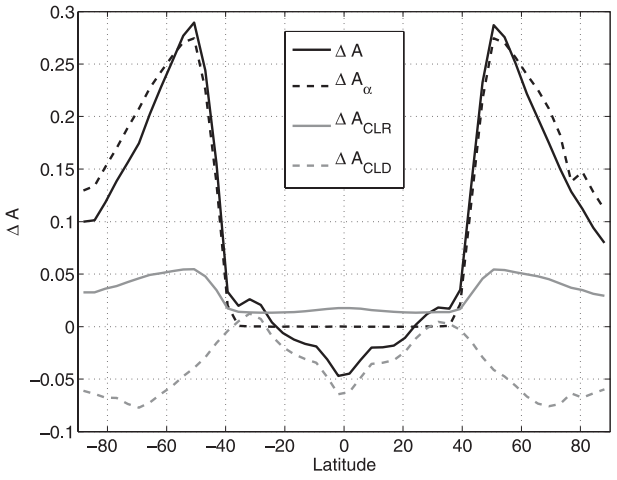

FIG. 7. Annually and zonally averaged change in TOA albedo between the cold and warm states of Ridge (ΔA; solid black) and contributions from surface albedo (ΔA_α; dashed black), cloud (ΔA_{CLD}; dashed gray), and noncloud (ΔA_{CLR}; solid gray) atmospheric radiative responses. See text for the details. The Aqua results are very similar.

temperature between the upper and lower limbs of the overturning circulation (see Czaja and Marshall 2006). This helps one rationalize changes in OHT on moving from the warm to the cold solutions: the OHT increases strongly in the subtropics but weakens at high latitudes, in both Ridge and Aqua. The first effect is primarily due to the strong cooling of the deep-water masses (which increases ΔT) and, to a lesser extent, the strengthening of the circulation (increase in Ψ). The effect is stronger in Aqua probably because its subtropical thermocline is very deep, extending down well in to the bottom waters. The second effect is related to the insulating role of sea ice:[7] at equilibrium, the OHT poleward of the sea ice edge must be very small.

The AHT also exhibits an increase in its peak value, consistent with a strengthening of the storm track from the warm to the cold state. Note that the increase is proportionally smaller than in the ocean. As a result, the total HT (Fig. 6, bottom) exhibits an increase over a broad band of latitudes. Interestingly, comparison of Ridge and Aqua emphasizes that the total HT is relatively insensitive to the details of the ocean–atmosphere circulation and depends primarily on the albedo, as discussed in Stone (1978) and Enderton and Marshall (2009).

The TOA albedo difference between the cold and warm states of Ridge is shown in Fig. 7, along with contributions from the surface albedo change and from changes in the cloud and noncloud radiative properties. The TOA (or planetary) albedo A is defined as $1 - Q/S$, where Q and S are the absorbed and total incoming solar radiation at the top of the atmosphere. Contributions to the TOA albedo change are computed following a modified version of the method described in Taylor et al. (2007, hereafter T07). More details are given in appendix B. The Aqua configuration gives similar results and is therefore not shown.

As expected from the sea ice cover expansion going from warm to cold states, the TOA albedo exhibits a large increase poleward of 40° (Fig. 7, solid black). The increase peaks at 0.28 near 55°, close to the ice edge, and decays to 0.1 at the poles. (The sharp decline seen on the equatorward side of 55° is in fact smoothed out by the zonal and annual averaging.) The TOA albedo increase averages to about 0.21 over the latitudes of the cold state sea ice cap (50°–90°). Gorodetskaya et al. (2006) estimated the impact of sea ice on TOA albedo from observations. They found an increase in TOA albedo of 0.25 (0.16) from ice-free to ice-covered conditions in the Northern (Southern) Hemisphere. Values from our GCM are consistent with these observational estimates.

The surface albedo contribution ΔA_α to the TOA albedo change (Fig. 7, dashed black) is by far the largest contribution. Importantly, note that the actual surface albedo change is about $2 \times \Delta A_\alpha$ (not shown). This shows that, regardless of the details of cloud cover and other atmospheric radiation conditions, the atmospheric opacity strongly attenuates the surface albedo changes when seen from the top of the atmosphere. The cloud contribution ΔA_{CLD} is negative nearly everywhere and is essentially due to a decrease in cloud cover in the drier cold state. On the other hand, the noncloud contribution is positive at all latitudes. This mainly results from a decrease in clear-sky atmospheric absorption in a drier climate (i.e., more shortwave passes through the drier atmosphere and bounces back to space). The cloud and noncloud contributions are small but not negligible. However, they tend to strongly compensate one another. As a consequence, the TOA albedo change appears, to first order, as a scaled down (by about a factor 2) surface albedo change. Note, however, that between 40°S and 40°N, where there is no surface albedo change, the cloud contribution dominates and leads to a small TOA albedo reduction.

A closer examination of the seasonal cycle of cloud cover (not shown) reveals that the largest differences between the warm and cold cases seen at high latitudes occur during the winter season. In the warm simulations with open, ice-free polar oceans, fractional cloud cover at high latitudes is high and relatively constant throughout the year, hovering near 85%. By contrast, the polar cloud cover in the cold simulations undergoes a large seasonal

[7] Note that vertical diffusion of heat across the ice layer is represented in the sea ice model and so it is not entirely insulating.

cycle, with summer values similar to the warm cases but winter values as low as 35%. The warm simulations thus experience an enhanced cloud cover during polar night relative to the ice-covered cases, and the additional infrared opacity of these clouds mitigates the winter season radiative cooling of the polar oceans. Clouds thus appear to contribute a positive feedback on temperature changes at high latitudes in this model. This effect is complementary to the ice albedo feedback but operates during the winter season when there is no albedo effect because of the polar darkness. It is reminiscent of the ''high-latitude convective cloud feedback'' described by Abbot and Tziperman (2008a,b), but the polar clouds in our model are not convective in origin. They appear to be driven by the large-scale atmospheric circulation and constrained by the very low moisture poleward of the sea ice edge in the cold simulations.

The increase of ASR and outgoing longwave radiation at the top of the atmosphere from cold to warm (Fig. 4, middle) partially cancel each other. The sign of the changes and their partial cancellation are not surprising as, moving from open ocean to sea ice–covered ocean, one expects less shortwave absorption and less thermal longwave emission (from the large temperature decrease throughout the atmosphere).

d. Variability of the coupled system

The mean states of the coupled system described above exhibit considerable internal variability on all time scales, from day-to-day variations, the seasonal cycle, and out to centennial fluctuations. Thus, the multiple states we have described are stable enough to persist through significant internal variability of the coupled system. This is important, because such variability is absent from the simplest EBMs, and the presence of noise has been shown to destabilize otherwise stable equilibria in some EBM solutions (Lee and North 1995). As expected, the largest perturbations occur on seasonal time scales. The seasonal and interannual variations of the Northern Hemisphere sea ice cover in the cold solutions are illustrated in Fig. 8. The climatological sea ice area varies by 14 million km^2 in Ridge and 7 million km^2 in Aqua over a season (20% and 10% of their annual-mean cover, respectively). Note that the sea ice covers are rather large relative to contemporary observations, because there is little land on our aquaplanets. The zonally averaged northern sea ice fraction at its maximum (January) and minimum (September) extent (Fig. 8, top right) gives an impression of the geographical variation of sea ice cover with the seasons. Note that the ice ''edge'' is in fact rather wide, notably at the maximum sea ice extent in January, with the ice fraction varying from 0% to 100% over 5°–10° of latitude. This is because the wintertime sea ice does not have time to reach full cover. In addition, for Ridge, there is a zonal asymmetry in the sea ice edge, which has a southwest-to-northeast tilt across the basin.

The annual-mean sea ice area anomalies for Ridge and Aqua are shown in Fig. 8 (bottom), for a stretch of 500 yr (note the absence of drift). In both solutions, anomalies of 2 million km^2 recur, sometimes persisting over a decade or more, with occasional excursions exceeding 3 million km^2. The Aqua time series is somewhat regular in behavior, and its spectrum has a marked peak at a 40-yr period. The Ridge time series has a more random behavior and a ''red noise'' spectrum.

e. Summary

The key characteristics of the multiple states described above are summarized in the schematic diagram (Fig. 9). It shows the ocean's thermocline, residual circulation, OHT, and sea ice extent in the warm, cold, and snowball states. The latitude of 50° corresponds (approximately) to the poleward edge of the subtropical thermocline set by the pattern of prevailing winds. Because the multiple equilibria exist in both Ridge and Aqua, the schematic emphasizes their common aspects.

As noted above, the ''bulge'' of the warm subtropical thermocline is a consequence of Ekman pumping associated with the trade/westerly winds acting at the surface. It is also the location of the bulk of the OHT, which is primarily achieved by a wind-driven meridional overturning circulation (blue). Poleward of the subtropical thermocline, the OHT drops to vanishingly small values. Hence, heat is ''deposited'' at the poleward edge of the subtropical thermocline, which also corresponds to the mean location of the ice edge in the cold solution. It appears then that convergence of OHT on the poleward flank of the subtropical thermocline limits the equatorial expansion of sea ice, leading to a stable equilibrium with a large polar ice cap.

Despite large differences in the ocean dynamics due to the very different geometrical constraints in Aqua and Ridge, the wind-driven subtropical cell dominates the OHT, resulting in a large midlatitude OHT convergence in all cases. Note that the difference in OHT between the cold and warm states seems to be of secondary importance because they both realize a large midlatitude OHT convergence.

4. Slab ocean experiments with specified OHT

To further explore the role of OHT, we present a series of experiments with our coupled system in which the ocean component is replaced by a slab-mixed layer of uniform depth with prescribed OHT convergence or ''q flux.'' The atmosphere and sea ice components are

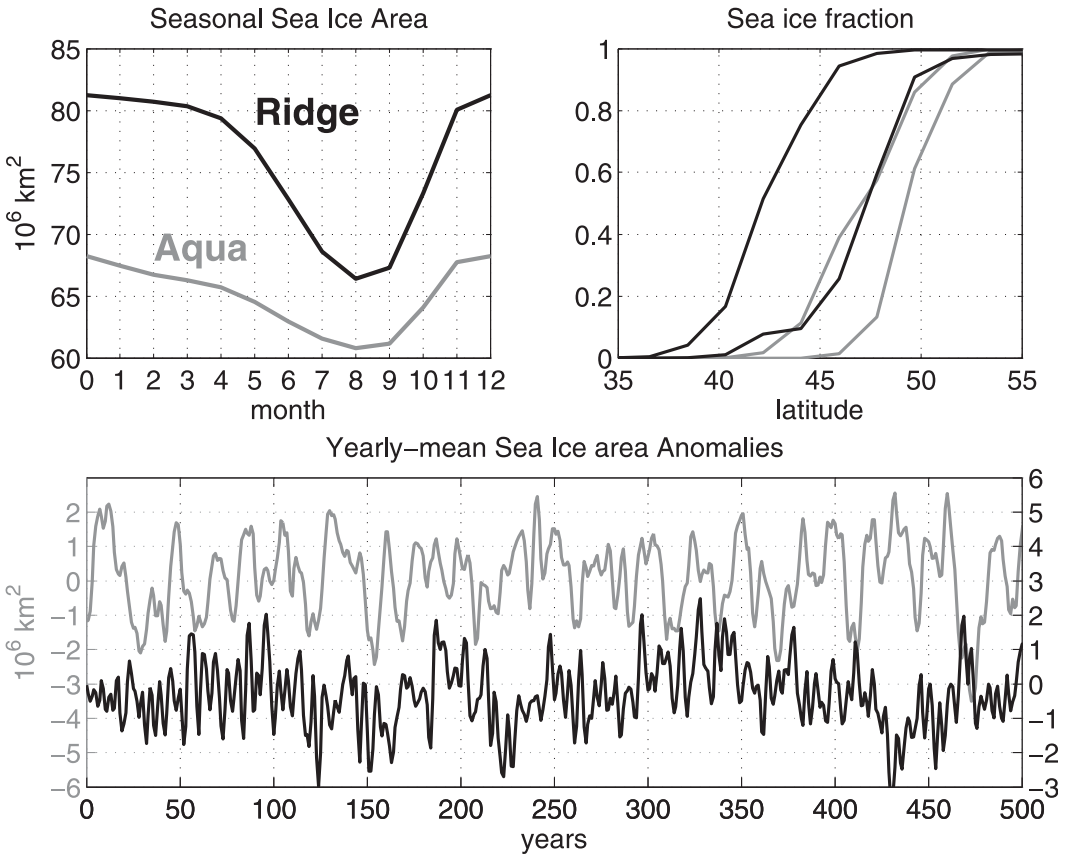

FIG. 8. (top left) Seasonal cycle of the Northern Hemisphere sea ice extent (10^6 km^2). (top right) Zonal-mean Northern Hemisphere sea ice concentration in January and September. (bottom) Annual-mean sea ice extent anomaly in the Northern Hemisphere as a function of time (note that, to remove some of the highest frequencies, the time series are smoothed with a 1–2-1 running mean filter). Black and gray curves correspond to Ridge and Aqua, respectively.

identical to those used in the coupled GCM while, in the ocean, the SST is now the only prognostic variable. Climatological monthly-mean heat budgets of the top ocean level are used to diagnose the q flux for both the warm and cold equilibrium states. Annual and zonal means of the q flux are plotted in Fig. 10 (left).

A first set of experiments is realized with this system by initializing it from the cold and warm states of the coupled GCM and applying the warm and cold q fluxes. All experiments are integrated out to equilibrium: 100 yr is sufficient in most cases. We use a mixed layer depth of 30 m (the thickness of the first ocean level of the coupled model); other choices of mixed layer depths yield different adjustment times but do not produce a different equilibrium. The time evolution of the sea ice extent for the four runs is shown in Fig. 10 (right). It is plotted in terms of an equivalent ice-edge latitude defined as the latitude of the sea ice caps if they were zonally and interhemispherically symmetric (this diagnostic effectively smoothes out seasonal variations).

We also carry out a set of perturbation experiments in which the q flux is slightly modified so as to move its peak value meridionally. The perturbations are dipoles with Gaussian-shaped lobes of amplitude ± 8 W m^{-2}. The perturbations are steady state (no seasonal component) and preserve the globally integrated ocean heat budget. For each q flux, both positively and negatively perturbed q fluxes are constructed, corresponding to a poleward and an equatorward displacement of the OHT convergence, respectively (shown in color shading in Fig. 10, left). The perturbation experiments are started from the equilibrium states of the unperturbed experiments and are shown in Fig. 10 (right, years 100–200; the color coding of the curves matches that of the perturbed q flux shown on the left).

To build our confidence in the relevance of the slab-ocean model, it is notable that it reproduces the fully coupled GCM equilibrium states. When the warm initial conditions and q flux are paired, the solution equilibrates into a nearly ice-free state (upper red curve at right panel). For the cold pairing, the solution has a sea ice cap

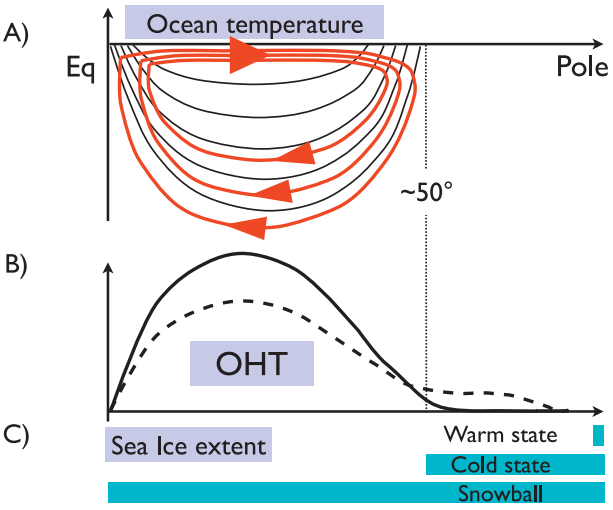

FIG. 9. Schematic of the multiple equilibrium states: (a) ocean thermal structure (black) and residual overturning circulation (red), (b) OHT transport in the warm (dashed) and cold (solid) states, and (c) sea ice extent for the three stable states.

extending into the midlatitudes around 50° (lower blue curve).

If now the cold q flux case is run from the warm state, the solution remains ice free (upper blue curve). Conversely, if the warm q flux is employed with cold state initial conditions, the large ice cap persists, although it expands equatorward by 15° of latitude. This is not unexpected in the light of the scenario described in Fig. 9: the region of strong OHT convergence occurs at a lower latitude in the warm state (Fig. 6, left). A further test can be seen in the perturbation experiments with large ice caps. For both warm and cold q flux, a positive (negative) perturbation—a slight poleward (equatorward) shift of the peak convergence—results in a poleward (equatorward) shift of the ice edge. On the other hand, the ice-free solutions are completely insensitive to the q-flux perturbations. This is not surprising, because the ice-free state is not sensitive to the difference between the warm and cold q fluxes.

We have also experimented with simple analytical forms for the q flux and found that, when the OHT has a broad equator-to-pole structure (as seen in classical EBMs) rather than a strong midlatitude convergence, the large ice cap solution does not exist. We are currently investigating these issues in more detail (B. Rose 2011, unpublished manuscript).

These slab-ocean experiments confirm that the existence of the multiple states (a large ice cap and an ice-free state) is made possible by the meridional structure of the OHT, namely a large OHT out of the tropics and a relatively weak transport at high latitudes. Importantly, the existence of the multiples states does not depend on the details of the OHT structure, although the exact location of the edge of the large ice cap does. Furthermore, our results support the interpretation of the mechanism at work in the coupled GCM sketched in Fig. 9. In the cold states, the ice edge equilibrates just poleward of the maximum

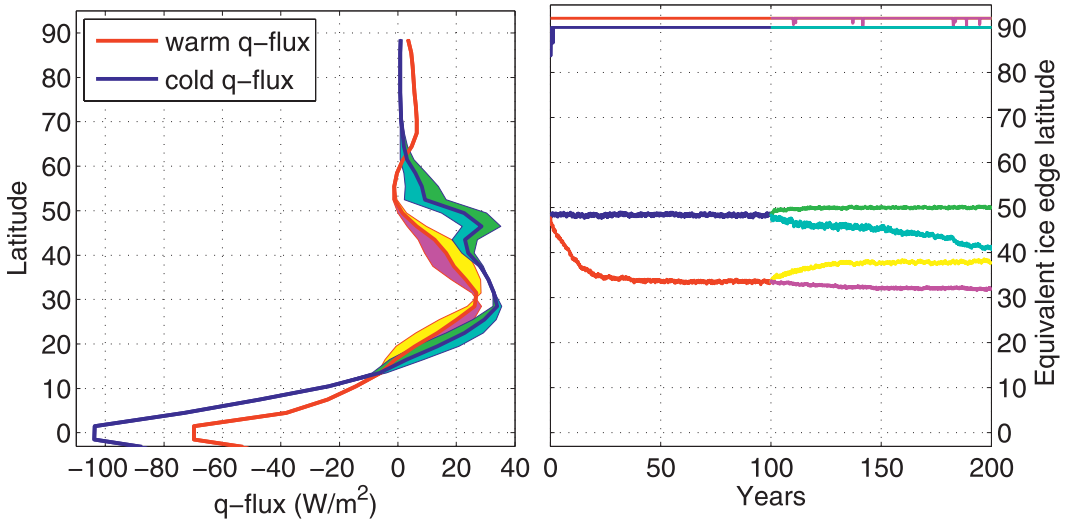

FIG. 10. Results from atmosphere-slab ocean runs with specified OHT. (left) Mean q fluxes diagnosed from the warm (red) and cold (blue) states of Aqua. The green and yellow shadings indicate positively perturbed q fluxes (i.e., poleward migration of the OHT convergence), while the cyan and magenta shadings indicate negatively perturbed q fluxes (i.e., equatorward migration of the OHT convergence). (right) Time series of the equivalent sea ice latitude (see text) starting from the warm (equivalent latitude of ~90°) and cold (equivalent latitude of ~50°) states of the coupled GCM. The perturbed experiments are started from the equilibrated states of the unperturbed experiments and are displayed for years 100–200. The color coding of the curves corresponds to that used for the q flux in (left).

OHT convergence. We take this as strong evidence that OHT convergence stabilizes the ice edge, preventing further equatorward migration.

5. Interpretation of multiple equilibria in terms of an energy balance model

Building on the sketch shown in Fig. 9, we now explore a modified version of the ocean–atmosphere–sea ice EBM developed by RM09. The RM09 model extends the classical EBM in two important ways: 1) the temperature and heat transport of the two fluids (atmosphere and ocean) are represented explicitly and 2) the effect of sea ice is represented not only in the surface albedo but also in the insulation of the ocean/atmosphere interface. This framework allows RM09 to explore the consequences of latitudinal structure of the OHT. They demonstrate the existence of an additional stable equilibrium state (not present in the classic EBM) in which the ice edge prefers to rest at latitudes where OHT reaches a minimum. Their model thus requires a stronger constraint on OHT than seen here in our coupled GCM.

The RM09 model employs gyre dynamics as a ''proxy'' to explore the impact of latitudinal structure of the OHT on the multiple equilibria. Diagnostics of our coupled GCM, however, shows that the wind-driven meridional overturning circulation is the principal agent of OHT rather than horizontal gyres (which are, of course, entirely absent in Aqua). Here, therefore, we modify the RM09 EBM to take into account the dynamics seen in the coupled model: that is, an OHT dominated by wind-driven subtropical overturning cells acting on a vertical temperature gradient. In the following, we show that, by using such a representation of the OHT, RM09's EBM supports multiple equilibria, which bear a marked similarity with those seen in the coupled GCM.

a. Formulation of atmosphere–ocean EBM

The atmosphere–ocean EBM (AO-EBM) used here is identical to that of RM09, with the exception of the different treatment of the ocean dynamics. The reader is thus referred to RM09 for a detailed description.

The model consists of two coupled, zonally averaged heat-budget equations governing the atmosphere and ocean through temperatures T_a and T_s (functions of latitude ϕ and time). We account for annual-mean solar heating, emissions to space, air–sea heat exchange, and convergence of heat transport in each fluid as follows:

$$C_a \frac{\partial T_a}{\partial t} = -\frac{1}{2\pi a^2 \cos\phi}\frac{\partial \mathcal{H}_a}{\partial \phi} + F_{\text{up}} - F_{\text{out}} \quad \text{and} \quad (1)$$

$$C_o \frac{\partial T_s}{\partial t} = -\frac{1}{2\pi a^2 \cos\phi}\frac{\partial \mathcal{H}_o}{\partial \phi} + \frac{S_o}{4}\mathcal{A}s(\phi) - F_{\text{up}}. \quad (2)$$

Here, $C_{a/o}$ are column-integrated heat capacities (J m^{-2} °C^{-1}), $\mathcal{A}$ is the coalbedo, S_o is the solar constant, $s(\phi)$ is a specified latitudinal distribution of solar heating, $F_{\text{out}} = A_{\text{out}} + B_{\text{out}}T_a$ is the outgoing longwave flux, $F_{\text{up}} = A_{\text{up}} + B_{\text{up}}(T_s - T_a)$ is the net surface-to-atmosphere heat flux, $\mathcal{H}_{a/o}$ are the heat transport terms (W), and a is the planetary radius. In the model, T_s represents the temperature of the surface, which may be open water or sea ice. The ice–albedo feedback is included by allowing $\mathcal{A}$ to drop discontinuously where T_s reaches the freezing threshold T_f.

The AHT is treated as a simple diffusion down the mean temperature gradient,

$$\mathcal{H}_a = -2\pi \cos\phi C_a K_a \frac{\partial T_a}{\partial \phi}. \quad (3)$$

Here, the coefficient K_a is taken as constant in latitude.

b. Representation of ocean heat transport

To capture the OHT dynamics seen in the GCM, we parameterize $\mathcal{H}_o$ as the sum of a meridional overturning acting on a vertical temperature gradient and a diffusive term,

$$\mathcal{H}_o = 2\pi a \cos\phi C_o\left(\psi_{\text{res}}\frac{T_s - T_{\text{deep}}}{\Delta z} - \frac{K_o}{a}\frac{\partial T_s}{\partial \phi}\right), \quad (4)$$

where ψ_{res} is a prescribed overturning streamfunction, T_{deep} is the deep-ocean temperature, and Δz is a depth scale over which the overturning is assumed to operate. In contrast to RM09, the diffusion coefficient K_o is constant and small. Diffusion is included primarily to satisfy boundary conditions: its contribution to OHT is small relative to that of the ψ_{res} term. The spatial structure in OHT is introduced through ψ_{res}, which has a prescribed latitudinal structure.

As seen in Fig. 5 and discussed in section 3b, deep-ocean temperatures in the coupled GCM are spatially homogeneous in all four states, roughly equal to the surface temperature near 50°–55°. We formalize this in the EBM by setting T_{deep} equal to the surface ocean temperature at a specified critical latitude ϕ_{crit} (which we take as 50°),

$$T_{\text{deep}} = \max[T_s(\phi_{\text{crit}}), T_f]. \quad (5)$$

Note that the max operator appears here because, where there is sea ice cover, T_s represents the ice-top temperature, whereas the ocean temperature below the ice is assumed to be T_f. The vertical temperature gradient

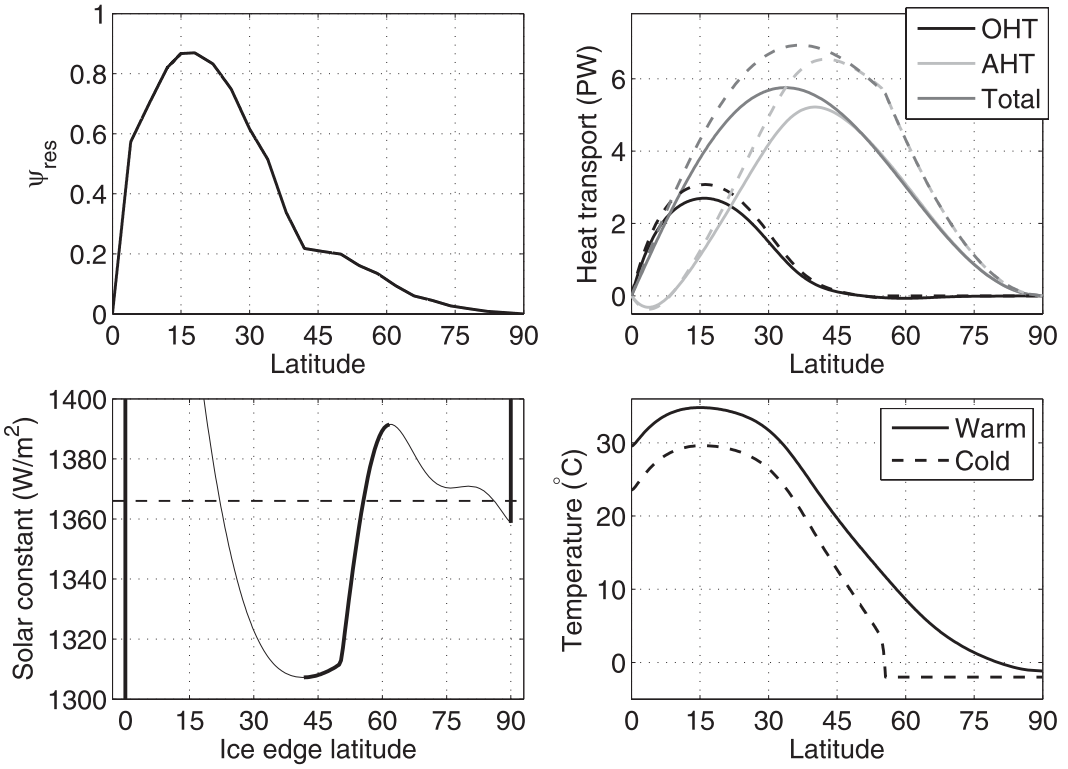

FIG. 11. Results of the modified AO-EBM of RM09. (top left) Profile of ocean overturning in potential temperature coordinates diagnosed from the warm Aqua state. This profile is used to parameterize the OHT $\mathcal{H}_o$ [see Eq. (4)]. (bottom left) Hysteresis plot showing the ice-edge latitude of the steady-state solution of the AO-EBM. Stable (unstable) solutions are denoted by thick (thin) lines. The dashed line indicates $S_o = 1366$ W m^{-2}. (top right) Oceanic, atmospheric, and total heat transports and (bottom right) SST profiles of the cold (dashed) and warm (solid) solutions obtained for $S_o = 1366$ W m^{-2}.

$T_s - T_{\text{deep}}$ thus changes sign across ϕ_{crit}, in agreement with the GCM results.

The formulation of the overturning contribution to the OHT in Eq. (4) makes it clear that, in essence, the term $\psi_{\text{res}}/\Delta z$ is the overturning streamfunction computed in temperature layers. Such ideas have been used to explore the partitioning of the ocean and atmosphere heat transport (e.g., Held 2001; Czaja and Marshall 2006). Here, we computed the overturning streamfunction in potential temperature layers from Aqua (not shown here; for plots and details, see Marshall et al. 2007). This overturning is comprised of two antisymmetric cells, not unlike the z-coordinate MOC shown in Fig. 5. The magnitude of the cell as a function of latitude is plotted in Fig. 11 (top left). Here, ψ_{res} rises from zero at the equator to a large tropical peak, falls off rapidly in the subtropics, and decays more gradually into the higher latitudes. When multiplied by the vertical temperature gradient, this produces a large OHT out of the tropics and much more modest extratropical OHT, in accordance with the coupled GCM shown in Fig. 6. In our calculations, ψ_{res} is held constant. Note, however, that the OHT is a prognostic variable in our EBM because both T_s and T_{deep} are free to evolve.

We set the time derivatives of Eqs. (1)–(2) to zero and solve the EBM as a numerical boundary value problem. This is a numerical generalization of the analytical method described by North (1975) for the classical EBM. No-flux conditions are imposed at the equator and pole. Continuity conditions are imposed on T_a and $\mathcal{H}_a$ at the ice edge. For the ocean, we impose $T_s = T_f$ and $\mathcal{H}_o = 0$ at the ice edge. This no-flux condition represents the insulating effect of the sea ice as described in RM09. This method maps out the entire solution space of the EBM, including both stable and unstable branches. This approach differs from RM09, who used a time-stepping procedure to solve Eqs. (1)–(2) and thus found only stable states.

Parameter values for the EBM calculations are given in Table 2; they are chosen to give a good fit between the warm states of the EBM and the coupled GCM. In particular, the radiative and albedo parameters allow for good quantitative agreement in both the shortwave and longwave budgets at the top of the atmosphere, thus

TABLE 2. Parameter values for the AO-EBM calculations. See RM09 for complete symbol definitions.

Parameter	Value	Notes
a	6.373×10^6 m	The earth's radius
T_f	-2°C	Freezing temperature
a_0	0.72	Open-ocean coalbedo
a_2	-0.078	Open-ocean coalbedo (zenith angle dependence)
a_i	0.4	Ice-covered coalbedo
C_a	10^7 J m^{-2} °C^{-1}	Column-integrated heat capacity for the atmosphere
C_o	18.5×10^7 J m^{-2} °C^{-1}	Ocean heat capacity (mixed layer depth of 45 m)
K_a	4.0×10^6 m^2 s^{-1}	Atmospheric diffusivity
K_o	300 m^2 s^{-1}	Oceanic diffusivity
A_{out}	212 W m^{-2}	Outgoing longwave constant
B_{out}	1.5 W m^{-2} °C^{-1}	Outgoing longwave sensitivity
A_{up}	238 W m^{-2}	Surface heat flux constant
B_{up}	15 W m^{-2} °C^{-1}	Surface heat flux sensitivity

capturing the net effects of clouds in the coupled GCM. Let us emphasize that the EBM parameters were chosen ''by hand'' rather than a formal optimization procedure and that they were fitted only to the warm Aqua state.

c. *Equilibrium solutions of EBM*

There are three stable solutions to the EBM for the same parameters and external forcing, analogous to the three stable solutions seen in the coupled GCM. These are 1) a warm ice-free state, 2) a completely ice-covered snowball state, and 3) a cold state with a large ice cap extending down in to the midlatitudes. Figure 11 shows the SST (bottom right) and heat transports (top right) for the warm and cold states. The snowball solution, which is of little interest here, is not shown in detail.

The warm and cold solutions share many features with those seen in the coupled GCM for both Aqua and Ridge. The patterns of the heat transports are well captured. In particular, note the increase in subtropical OHT and its decrease at high latitudes on moving from the warm to the cold states. The total heat transport increases by about 1 PW at its peak going from warm to cold, as in the GCM. In both models, this increase largely consists of an increase in AHT, although the EBM shows a poleward shift in the peak AHT from warm to cold, which is not seen in the coupled GCM. This may be a consequence of the absence of atmospheric dynamics in the EBM or of our assumption of a fixed ψ_{res}.

The multiple-valued structure of the EBM solutions can be seen in the bottom-left panel of Fig. 11, where we plot the ice-edge latitude ϕ_i as a function of S_o. Branches of the curve where $d\phi_i/dS_o < 0$ (shown in thin lines) are unstable (Cahalan and North 1979). Multiple equilibria of interest are denoted by the intersections of this curve with the horizontal dashed line at the reference value $S_o = 1366$ W m^{-2}. With this parameter set, the three stable solutions coexist for a range of solar constants between 1360 and 1390 W m^{-2}. This figure shows that an abrupt transition from the warm to the cold state can be initiated by a modest ($\sim$6 W m^{-2}) reduction in solar constant from its reference value. The cold state is stable for S_o as low as 1310 W m^{-2}; the transition into the snowball state therefore requires a much larger reduction in S_o (about 4% of the reference value). The transition from cold to warm state is also abrupt in the EBM and occurs at $S_o = 1390$ W m^{-2}. We are currently investigating the extent to which the transitions between the warm and cold states in the coupled GCM resemble the EBM hysteresis curve in Fig. 11.

The existence of the cold state in the EBM, as well as its broad similarity to the cold state of the GCM, suggests that our simple EBM captures the important physics of the problem. As emphasized in RM09, the meridional structure of the OHT is a key to the stabilization of the midlatitude ice edge and thus the existence of multiple equilibria in the EBM and, we believe, in the much more complex coupled GCM.

6. Conclusions

We have shown that genuine multiple equilibria exist in a highly complex coupled ocean–atmosphere–sea ice model. In both Aqua and Ridge configurations, comprising very different ocean circulations, three different stable climate states are possible for exactly the same external forcing: a warm ice-free state, a cold state with an ice cap extending down into middle latitudes, and a snowball state in which the planet is entirely covered with ice. These states have very different climates, which persist for thousands of years without any hint of drift. Moreover, they exist in the presence of significant internal variability in the coupled system, an aspect that is conspicuously absent from, for example, EBMs: there is a seasonal cycle, weather noise, and vigorous internal variability on all time scales. Significantly, these multiple equilibria are not an

exotic feature of our coupled model obtained in only a narrow region of parameter space. They exist for different ice albedo parameters (appendix A), with or without sea ice thickness diffusion, and are found in two ocean geometries with very different ocean dynamics.

The warm state and the snowball state are perhaps not surprising, being the key prediction of classic EBMs. However, our coupled system also supports a third stable cold solution with an ice cap extending down in to middle latitudes. This new third stable state was anticipated by RM09. They showed that if EBMs are extended to take into account (i) the meridional structure of OHT and (ii) the insulating property of sea ice: a stable cold state with a large ice cap can be supported, in addition to the warm state and the snowball. Building on RM09, we showed that an EBM can capture the essential physics, generating three stable states that are very similar to those obtained in our complex coupled model.

The results of the coupled model, atmosphere-slab ocean model and EBM all suggest that the existence of three multiple states, and most notably of the equilibrium state with a large sea ice cap extending into the midlatitude is due to the meridional structure of the OHT. The key aspect is a strong convergence of OHT in to the midlatitudes from the tropics, as sketched in Fig. 9. Details of the meridional OHT structure do not matter for the existence of the multiple states. This is exemplified by the difference in OHT between Aqua and Ridge and by the atmosphere-slab ocean experiments. Let us emphasize that the condition for three multiple states is more general than put forward by RM09, who stressed the need for a minima in OHT: the Aqua setup does not have a local minimum in OHT. Indeed such dynamical features as gyre dynamics and polar deep convection (not found in Aqua but responsible for the secondary peak in OHT seen in Ridge) are not essential to support the cold state. Encouragingly, the existence of multiple equilibria appears to rely on rather robust dynamical features as 1) a wind-driven overturning cell that, overlaid on a subtropical thermocline, generates a large OHT in the subtropics and 2) a comparatively small OHT poleward of the subtropical thermocline. Both are robust features of the observed climate, even when considering the large uncertainties in observed OHT (Trenberth and Caron 2001; Wunsch 2005). They are also common features of Intergovernmental Panel on Climate Change (IPCC) class models under preindustrial conditions and global warming conditions (Randall et al. 2007). In addition, they are seen in other idealized configurations with north–south asymmetries and multiple basins (see Fig. 1 of Ferreira et al. 2010).

This leads us to believe that the highly idealized geometries employed here are not crucial to the existence of the multiple states. Nevertheless, much needs to be explored. Although our results prove that multiple states are not just a propriety of low-order models, the impact of the symmetric setup around the equator, of the absence of significant continental surfaces, and of the flat ocean bottom should all be evaluated. Explorations of multiple equilibria in the Double-Drake setup, which has interhemispheric asymmetries and multiple basins (Ferreira et al. 2010), are currently underway. In addition, although our coupled GCM has a full 3D dynamics in both ocean and atmosphere, much ground remains to be covered to reach the full complexity and resolution of IPCC class coupled models. Notably, our intermediate complexity atmospheric physics used in combination with low vertical resolution needs further inquiry.

Finally, it is worth putting our results in perspective with some paleoclimate records. The SST characteristics of the multiple states are reminiscent of those estimated for past climates such as the warm house of the Eocene and Cretaceaous and the Last Glacial Maximum (LGM). The warm solutions are also characterized by abyssal ocean temperatures, which reach ~12°C, not unlike those suggested by the paleo δ^{18}O record of 50 Ma (Miller et al. 1987). The SST increases from the cold to the warm state by 8°–9°C near the equator and by as much as to 35°–37°C at the poles (Fig. 4). The equator-to-pole temperature difference is large in the cold solutions, about 55°C, but decreases dramatically by a factor 2 (~28°C) in the warm solutions. These changes are as large as major climate shifts between the ice house of the LGM and the warm house climate of the Eocene (Pierrehumbert 2002).

These similarities raise the intriguing possibility that multiple states could exist in the real coupled climate system and furthermore that they could have played a role in past (and future) climatic evolution. This also raises the important question of how the system can transition between states. The inner variability of the coupled ocean–atmosphere–sea ice system appears unlikely to trigger transitions, at least in our configuration.[8] One has therefore to invoke (slowly) varying external

[8] Adkins et al. (2005) show that a stable stratification comprising fresh/cold on top of salty/warm water, as in our warm solutions, can store large amounts of potential energy because of the thermobaricity of seawater. If heated from below (e.g., by geothermal heating), such a state could become unstable and result in a catastrophic overturning event. If this were to happen to a warm state, relatively cold (but well above freezing point) surface water would be mixed with warmer deep water. This mechanism seems therefore unlikely to flip a warm state into a cold one. Furthermore, if one assumes a geothermal flux of 100 mW m^2 (a rather high value), the stratifications in Ridge and Aqua would take ~4000 and ~1300 yr, respectively, to become unstable in the absence of any diffusion or advection.

forcings such as orbital parameters and CO_2 concentrations. What are the magnitude and duration of the perturbations necessary to push the system from one state to the other and what are the time scales of those transitions? Can Aqua and Ridge, if appropriately forced, generate the characteristic sawtooth shape seen in glacial–interglacial cycle? We are currently investigating these issues.

Acknowledgments. The authors would like to acknowledge the Physical Oceanography division of the NSF for their support of this work. We also would like to thank the three anonymous reviewers, whose comments helped improve this manuscript.

APPENDIX A

Sea Ice Albedo Parameterization

Because of the key role of the snow/ice albedo in the multiple states, we briefly describe its representation in our GCM. The albedo has two contributions, from snow and ice. The ice albedo α_I has a minimum value of $\alpha_I^{\min}$ and increases with the sea ice thickness (exponentially on a thickness scale $h_I^{\alpha} = 0.25$ m) toward a maximum value $\alpha_I^{\max}$. The snow albedo α_S computation starts with a temperature dependence: the snow albedo is high α_S^{cold} for surface temperature lower than −5°C and decreases linearly to a low value α_S^{warm} for surface temperature higher than 0°C. The albedo thus obtained is lowered by an age dependence: an exponential decay on an ''age'' scale of 5 days toward α_S^{old}. The final snow/ice albedo is a weighted mean of α_S and α_I: $\alpha_I \exp(-h_S/h_S^{\alpha}) + \alpha_S[1 - \exp(-h_S/h_S^{\alpha})]$, where h_S is the snow layer thickness and $h_S^{\alpha} = 5$ cm.

The snow/ice albedo reaches its highest α_S^{cold} for a cold thick layer of fresh snow and its lowest value $\alpha_I^{\min}$ for a thin layer of bare ice. Importantly, note that the albedo of a surface grid cell is a weighted mean (by the sea ice fraction) of the snow/ice albedo and ocean albedo. Albedo parameters differing between Aqua and Ridge are given in Table 1.

APPENDIX B

Estimations of the Planetary Albedo Contributions

To estimate the contribution of surface albedo, cloud, and noncloud effects on differences in planetary albedo between states, we apply the ''approximate partial radiative perturbation'' procedure described in T07. The method is based on a simple shortwave radiative model, which represents the full complexity of the atmosphere by means of three parameters: a surface albedo α, an atmospheric absorption μ, and an atmospheric scattering γ. Using outputs from the GCM, these coefficients are diagnosed for overcast and clear-sky portions of each model grid cell (in both the warm and cold states). Using the analytical expression for the planetary albedo A, one can then estimate its various contributions by ''plugging in'' the relevant cold and warm parameters and differentiate.

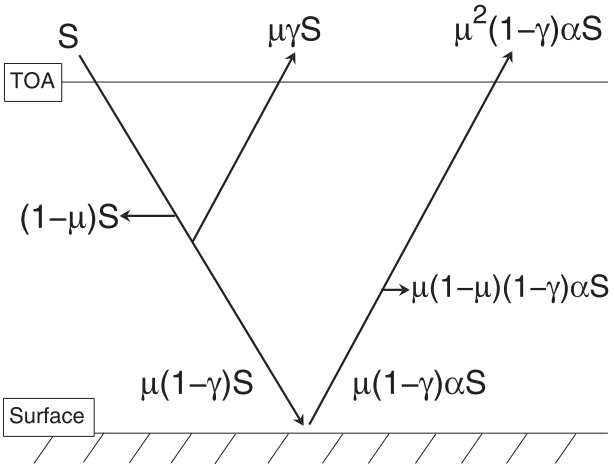

FIG. B1. Schematic of the simple shortwave radiative model used with the methodology of T07. The model represents a pass of a shortwave beam up and down the atmosphere: S is the solar insolation, γ is the scattering coefficient, $(1 - \mu)$ is the atmospheric absorption, and α is the surface albedo. Note that absorption occurs both in the downwelling and upwelling branches, but there is scattering only in the downwelling pass.

Here, we find that use of the shortwave model described in T07 leads to unphysical results (e.g., negative atmospheric absorption under clear-sky conditions). Therefore, we modify the simple shortwave radiative model so that it parallels more closely the actual computation carried in the coupled GCM. Except for this modification, we follow the method described in T07.

In our shortwave radiative model, a shortwave beam does a single pass up and down the atmosphere (see Fig. B1 for a schematic). It is modified successively by absorption and scattering back to space on the downward path, reflection at the ground, and absorption on the upward path. We define A as $1 - Q/S$, where S and Q are the total incoming and absorbed solar radiation at the top of the atmosphere, respectively. Also, we have the following:

$$Q_s^{\downarrow} = \mu(1 - \gamma), \tag{B1}$$

$$Q_s^{\uparrow} = \mu(1 - \gamma)\alpha, \quad \text{and} \tag{B2}$$

$$Q_t^{\uparrow} = \mu\gamma + \mu^2(1 - \gamma)\alpha, \tag{B3}$$

where $Q_s^{\downarrow}$, $Q_s^{\uparrow}$, and $Q_t^{\uparrow}$ are the surface downward, surface upward, and TOA upward shortwave fluxes divided by S. After some simple manipulations, one obtains the following:

$$\alpha = \frac{Q_s^{\uparrow}}{Q_s^{\downarrow}}, \tag{B4}$$

$$\gamma = \frac{Q_t^{\uparrow} - Q_s^{\uparrow} Q_s^{\downarrow}}{Q_s^{\downarrow} + Q_t^{\uparrow}}, \quad \text{and} \tag{B5}$$

$$\mu = \frac{Q_s^{\downarrow}}{1 - \gamma}. \tag{B6}$$

Finally, the TOA albedo can also be expressed as

$$A(\mu, \gamma, \alpha) = 1 - \frac{Q}{S} = \mu\gamma + \mu^2(1 - \gamma)\alpha. \tag{B7}$$

One can, for example, estimate the surface albedo contribution to the TOA albedo change between the cold and warm states as [see Eq. (12b) of T07]

$$\Delta A_{\alpha} = \frac{1}{2}[A(\mu_c, \gamma_c, \alpha_c) - A(\mu_c, \gamma_c, \alpha_w)] + \frac{1}{2}[A(\mu_w, \gamma_w, \alpha_c) - A(\mu_w, \gamma_w, \alpha_w)], \tag{B8}$$

where the subscripts "w" and "c" denote parameters estimated from Eqs. (B4)–(B6) for the warm and cold states, respectively. We refer the reader to T07 for more details [particularly Eqs. (16b) and (16c)], which gives contributions from cloud and noncloud atmospheric radiative properties to the TOA albedo change). Note that, as in T07, we use climatological monthly-mean fields to compute all quantities, which are then annually and zonally averaged (Fig. 7).

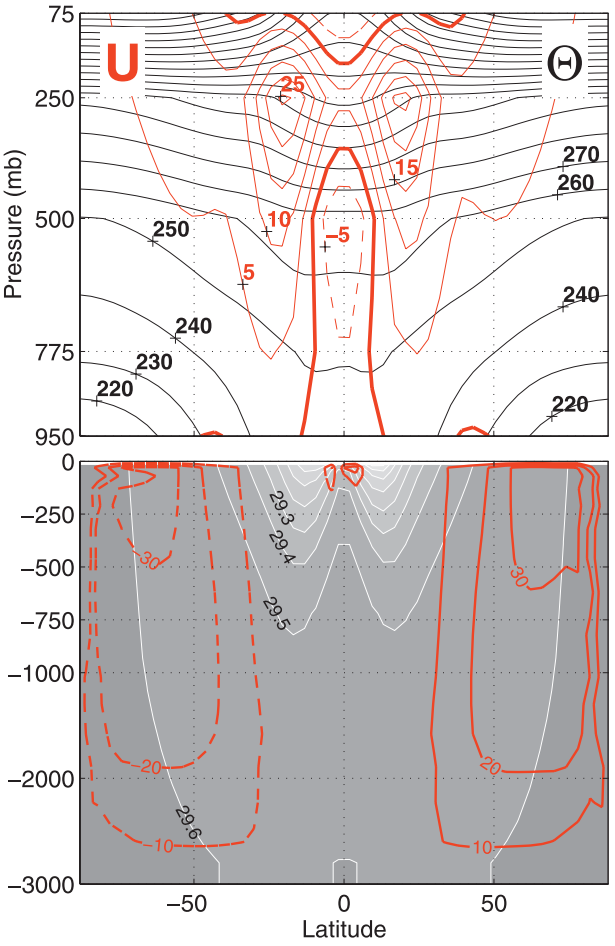

FIG. C1. The snowball solution in Aqua: (top) zonal-mean potential temperature (black; K) and zonal wind (red; m s^{-1}) in the atmosphere and (bottom) zonal-mean density (shaded) and residual-mean streamfunction (red; Sv) in the ocean.

APPENDIX C

Snowball Earth Solution

To explore the existence and nature of snowball solutions in Ridge and Aqua, the two configurations were initialized with uniform T and S in the ocean (S = 35 psu and $T = -1.9$°C, the freezing point of water at this salinity) and a uniform 10-m-thick sea ice sheet over the whole globe. From these initial conditions, the ocean in both configurations further cools while sea ice thickens. This happens because the water extracted from the ocean to grow sea ice increases the salinity and thus lowers the freezing point. After 2000 yr, the sea ice is about 200 m thick and, although the solutions are not equilibrated, the rate of cooling decreases. Goodman and Pierrehumbert (2003) suggest that sea ice thickness in a snowball world could grow in excess of a kilometer and that geothermal heating (as the only source of heat for the ocean) is a key factor in determining the equilibrium thickness. Finding equilibrated snowball solutions was not attempted here. Instead, we seek to demonstrate that, in both Ridge and Aqua, a snowball state coexists along with the warm and cold solutions for exactly the same set of parameters and external forcings.

The snowball solutions exhibit very interesting circulation patterns, as can be seen in Fig. C1 for the Aqua configuration after 2000 yr of integration (the Ridge snowball solution shows similar features). As shown in the top panel, the atmosphere is very cold, with small equator-to-pole gradients. This is to be expected, because most of the incoming solar radiation is radiated back to space. As a consequence of the small baroclinicity, there is little synoptic-scale activity and surface winds are close to zero. Moreover, the atmosphere is very dry, with

specific humidity reaching only 0.5 g kg^{-1} near the surface at the equator.

The sea ice reaches a maximum thickness of ~200 m at the pole decreasing to about 175 m at the equator. In the ocean, the temperature is nearly uniform, varying by a few hundredths of a degree around the mean value of −1.98°C. The (weak) density stratification is almost exclusively due to salinity contrast, itself resulting from freezing near the poles and melting of sea ice in the tropics. The freshwater budget is balanced by the action of sea ice thickness diffusion transferring ice from the pole to the equator. At the pole, brine rejection associated with freezing generates deep convection and the densest water masses.

As expected, the Eulerian circulation is close to zero, because there is little mechanical or buoyancy forcing at the top of the ocean (suggestive of the possible key role of geothermal heating). Interestingly, the eddy-induced circulation is the main component and is in fact of substantial magnitude, reaching 30 Sv (1 Sv $\equiv 10^6$ m^3 s^{-1}) at high latitudes. This circulation opposes the salt contrast generated by the pattern of freezing/melting, transporting freshwater from the tropics poleward. Note that ocean freshwater, ocean heat transport, and atmospheric heat transport are all very small, peaking at 0.09 Sv, 10^{-3} PW, and 0.4 PW, respectively.

REFERENCES

Abbot, D. S., and E. Tziperman, 2008a: A high-latitude convective cloud feedback and equable climates. *Quart. J. Roy. Meteor. Soc.,* **134,** 165–185.

——, and ——, 2008b: Sea ice, high-latitude convection, and equable climates. *Geophys. Res. Lett.,* **35,** L03702, doi:10.1029/2007GL032286.

Adcroft, A., and J.-M. Campin, 2004: Rescaled height coordinates for accurate representation of free-surface flows in ocean circulation models. *Ocean Modell.,* **7,** 269–284, doi:10.1016/j.ocemod.2003.09.003.

——, ——, C. Hill, and J. Marshall, 2004: Implementation of an atmosphere–ocean general circulation model on the expanded spherical cube. *Mon. Wea. Rev.,* **132,** 2845–2863.

Adkins, J., A. Ingersoll, and C. Pasquero, 2005: Rapid climate change and conditional instability of the glacial deep ocean from the thermobaric effect and geothermal heating. *Quat. Sci. Rev.,* **24,** 581–594.

Bitz, C., M. Holland, E. Hunke, and R. Moritz, 2005: Maintenance of the sea-ice edge. *J. Climate,* **18,** 2903–2921.

Broecker, W. S., D. M. Peteet, and D. Rind, 1985: Does the ocean-atmosphere system have more than one stable mode of operation? *Nature,* **315,** 21–26.

Bryan, F., 1986: High-latitude salinity effects and interhemispheric thermohaline circulation. *Nature,* **323,** 301–304.

Bryan, K., 1984: Accelerating the convergence to equilibrium of ocean climate models. *J. Phys. Oceanogr.,* **14,** 666–673.

Budyko, M., 1969: The effect of solar radiation variations on the climate of the earth. *Tellus,* **21,** 611–619.

Cahalan, R. F., and G. R. North, 1979: A stability theorem for energy-balance climate models. *J. Atmos. Sci.,* **36,** 1178–1188.

Campin, J.-M., J. Marshall, and D. Ferreira, 2008: Sea ice–ocean coupling using a rescaled vertical coordinate *z**. *Ocean Modell.,* **24,** 1–14, doi:10.1016/j.ocemod.2008.05.005.

Chamberlin, T. C., 1906: On a possible reversal of deep-sea circulation and its influence on geologic climates. *J. Geol.,* **14,** 363–373.

Claussen, M., 1998: On multiple solutions of the atmosphere-vegetation system in present-day climate. *Global Change Biol.,* **4,** 549–559.

Czaja, A., and J. Marshall, 2006: The partitioning of poleward heat transport between the atmosphere and the ocean. *J. Atmos. Sci.,* **63,** 1498–1511.

Enderton, D., and J. Marshall, 2009: Explorations of atmosphere–ocean–ice climates on an aquaplanet and their meridional energy transports. *J. Atmos. Sci.,* **66,** 1593–1611.

Ferreira, D., J. Marshall, and J.-M. Campin, 2010: Localization of deep water formation: Role of atmospheric moisture transport and geometrical constraints on ocean circulation. *J. Climate,* **23,** 1456–1476.

Gent, P. R., and J. C. McWilliams, 1990: Isopycnic mixing in ocean circulation models. *J. Phys. Oceanogr.,* **20,** 150–155.

Goodman, J. C., and R. T. Pierrehumbert, 2003: Glacial flow of floating marine ice in "Snowball Earth." *J. Geophys. Res.,* **108,** 3308, doi:10.1029/2002JC001471.

Gorodetskaya, I. V., M. A. Cane, L.-B. Tremblay, and A. Kaplan, 2006: The effects of sea-ice and land-snow concentrations on planetary albedo from the Earth Radiation Budget Experiment. *Atmos.–Ocean,* **44,** 195–205.

Held, I. M., 2001: The partitioning of the poleward energy transport between the tropical ocean and atmosphere. *J. Atmos. Sci.,* **56,** 1688–1697.

Hoffmann, P. F., A. J. Kaufman, G. P. Halverson, and D. P. Schrag, 1998: A Neoproterozoic Snowball Earth. *Science,* **281,** 1342–1346.

Jackett, D. R., and T. J. McDougall, 1995: Minimal adjustment to hydrographic profiles to achieve static stability. *J. Atmos. Oceanic Technol.,* **12,** 381–389.

Klinger, B. A., J. Marshall, and U. Send, 1996: Representation of convective plumes by vertical adjustment. *J. Geophys. Res.,* **101** (C8), 18 175–18 182.

Langen, P. L., and V. A. Alexeev, 2004: Multiple equilibria and asymmetric climates in the CCM3 coupled to an oceanic mixed layer with thermodynamic sea ice. *Geophys. Res. Lett.,* **31,** L04201, doi:10.1029/2003GL019039.

Lee, W.-H., and G. R. North, 1995: Small ice cap instability in the presence of fluctuations. *Climate Dyn.,* **11,** 242–246.

Lenton, T. M., H. Held, E. Kreigler, J. W. Hall, W. Lucht, S. Rahmstorf, and H. J. Schellnhuber, 2008: Tipping elements in the Earth's climate system. *Proc. Natl. Acad. Sci. USA,* **105,** 1786–1793.

Lorenz, E. N., 1968: Climate determinism. *Meteor. Monogr.,* No. 25, Amer. Meteor. Soc., 1–3.

——, 1970: Climate change as a mathematical problem. *J. Appl. Meteor.,* **9,** 325–329.

Manabe, S., and R. J. Stouffer, 1988: Two stable equilibria of a coupled ocean-atmosphere model. *J. Climate,* **1,** 841–866.

Marotzke, J., and M. Bozet, 2007: Present-day and ice-covered equilibrium states in a comprehensive climate model. *Geophys. Res. Lett.,* **34,** L16704, doi:10.1029/2006GL028880.

Marshall, J., and F. Schott, 1999: Open-ocean convection: Observations, theory, and models. *Rev. Geophys.,* **37,** 1–64.

——, and T. Radko, 2003: Residual-mean solutions for the Antarctic Circumpolar Current and its associated overturning circulation. *J. Phys. Oceanogr.,* **33,** 2341–2354.

——, A. Adcroft, C. Hill, L. Perelman, and C. Heisey, 1997a: A finite-volume, incompressible Navier Stokes model for studies of the ocean on parallel computers. *J. Geophys. Res.,* **102** (C3), 5753–5766.

——, C. Hill, L. Perelman, and A. Adcroft, 1997b: Hydrostatic, quasi-hydrostatic, and non-hydrostatic ocean modeling. *J. Geophys. Res.,* **102** (C3), 5733–5752.

——, A. Adcroft, J. M. Campin, C. Hill, and A. White, 2004: Atmosphere–ocean modeling exploiting fluid isomorphisms. *Mon. Wea. Rev.,* **132,** 2882–2894.

——, D. Ferreira, J. M. Campin, and D. Enderton, 2007: Mean climate and variability of the atmosphere and ocean on an aquaplanet. *J. Atmos. Sci.,* **64,** 4270–4286.

Miller, K. G., T. R. Janacek, M. E. Katz, and D. Keil, 1987: Abyssal circulation and benthic foraminiferal changes near the Paleocene/Eocene boundary. *Paleoceanography,* **2,** 741–761.

Molteni, F., 2003: Atmospheric simulations using a GCM with simplified physical parametrizations. I: Model climatology and variability in multi-decadal experiments. *Climate Dyn.,* **64,** 175–191, doi:10.1007/s00382-002-0268-2.

North, G. R., 1975: Analytical solution to a simple climate model with diffusive heat transport. *J. Atmos. Sci.,* **32,** 1301–1307.

——, R. F. Cahalan, and J. A. Coakley, 1981: Energy balance climate models. *Rev. Geophys. Space Phys.,* **19,** 91–121.

Pierrehumbert, R. T., 2002: The hydrologic cycle in deep time climate problems. *Nature,* **419,** 191–198.

Poulsen, C. J., R. T. Pierrehumbert, and R. L. Jacob, 2001: Impact of ocean dynamics on the simulation of the Neoproterozoic ''Snowball Earth.'' *Geophys. Res. Lett.,* **28,** 1575–1578.

Rahmstorf, S., 1995: Bifurcations of the Atlantic thermohaline circulation in response to changes in the hydrological cycle. *Nature,* **378,** 145–149.

——, and Coauthors, 2005: Thermohaline circulation hysteresis: A model intercomparison. *Geophys. Res. Lett.,* **32,** L23605, doi:10.1029/2005GL023655.

Randall, D. A., and Coauthors, 2007: Climate models and their evaluation. *Climate Change 2007: The Physical Science Basis,* S. Solomon et al., Eds., Cambridge University Press, 589–662.

Redi, M. H., 1982: Oceanic isopycnal mixing by coordinate rotation. *J. Phys. Oceanogr.,* **12,** 1154–1158.

Renssen, H., V. Brovkin, T. Fichefet, and H. Goose, 2003: Holocene climate instability during the termination of the African Humid Period. *Geophys. Res. Lett.,* **30,** 1184, doi:10.1029/2002GL016636.

Rose, B., and J. Marshall, 2009: Ocean heat transport, sea-ice and multiple climate states: Insights from energy balance models. *J. Atmos. Sci.,* **66,** 2828–2843.

Sellers, W. D., 1969: A global climatic model based on the energy balance of the earth-atmosphere system. *J. Appl. Meteor.,* **8,** 392–400.

Stocker, T. F., 1999: Abrupt climate changes: From the past to the future—A review. *Int. J. Earth Sci.,* **88,** 365–374.

Stommel, H., 1961: Thermohaline convection with two stable regimes of flow. *Tellus,* **13,** 224–230.

Stone, P. H., 1978: Constraints on the dynamical transports of energy on a spherical planet. *Dyn. Atmos. Oceans,* **2,** 123–139.

Stouffer, R. J., and Coauthors, 2006: Investigating the causes of the response of the thermohaline circulation to past and future climate changes. *J. Climate,* **19,** 1365–1387.

Taylor, K. E., M. Crucifix, P. Braconnot, C. D. Hewitt, C. Doutriaux, A. J. Broccoli, J. F. B. Mitchell, and M. J. Webb, 2007: Estimating shortwave radiative forcing and response in climate models. *J. Climate,* **20,** 2530–2543.

Trenberth, K. E., and J. M. Caron, 2001: Estimates of meridional atmosphere and ocean heat transports. *J. Climate,* **14,** 3433–3443.

Wang, G., and E. A. B. Eltahir, 2000: Ecosystem dynamics and the Sahel drought. *Geophys. Res. Lett.,* **27,** 795–798.

Winton, M., 2000: A reformulated three-layer sea ice model. *J. Atmos. Oceanic Technol.,* **17,** 525–531.

Wunsch, C., 2005: The total meridional heat flux and its oceanic and atmospheric partition. *J. Climate,* **18,** 4374–4380.

Zachos, J., M. Pagani, L. Sloan, E. Thomas, and K. Billups, 2001: Trends, rhythms, and aberrations in global climate 65 Ma to present. *Science,* **291,** 686–693.